Activation of Methane by U^+ Studied by Guided Ion Beam Tandem Mass Spectrometry and Quantum Chemistry

Satish Kumar,[1] P. B. Armentrout[1,*] and Wibe A. de Jong[2]

[1] Department of Chemistry, University of Utah, 315 S. 1400 E. Rm. 2020, Salt Lake City, Utah 84112, USA

[2] Lawrence Berkeley National Laboratory, One Cyclotron Road, Berkeley, California 94720, USA

*Corresponding author: armentrout@chem.utah.edu

Abstract: Reaction pathways of all products formed in the $U^+ + CH_4$ (CD_4) reaction were explored as a function of kinetic energy using guided ion beam tandem mass spectrometry (GIBMS) and quantum chemical calculations. UH^+, UC^+, UCH^+, UCH_2^+, and UCH_3^+ (and their perdeuterated analogues) are formed in endothermic reactions. In both systems, the UCH_2^+ (UCD_2^+) dehydrogenated product was the dominant product in the low-energy region, whereas the UH^+ (UD^+) hydride product became predominant at high energies. The kinetic energy behavior of the various products is consistent with a common intermediate of H-U^+-CH_3 (D-U^+-CD_3). The kinetic energy dependence of all product cross sections was modeled to obtain experimental bond dissociation energies at 0 K (in eV): D_0 (U^+-H) = 2.42 ± 0.10, D_0 (U^+-C) = 3.95 ± 0.12, D_0 (U^+-CH) = 4.91 ± 0.09, D_0 (U^+-CH_2) = 4.11 ± 0.04, and D_0 (U^+-CH_3) = 2.41 ± 0.09. Quantum chemical calculations using UCCSD(T) and UB3LYP approaches with the cc-pwCVXZ-PP basis set with MDF-60 pseudopotential for U^+ and the aug-cc-pCVXZ and aug-cc-pVXZ (X = T, Q) basis set for carbon and hydrogen, respectively, validate the experimental bond dissociation energies and outline the potential energy surface for all reactions observed. In addition, spin-orbit corrections of the bond energies for all products were calculated at a CASSCF-CASPT2-RASSI level.

Introduction

The activation of methane C-H bonds in catalysis is significant because of its importance in the industrial process of converting natural gas to more easily transportable liquid fuels.[1-4] Because it is relatively inert, methane must first be thermally cracked to form synthesis gas before it can be converted into synthetic fuels via the Fischer−Tropsch process employing Fe- or Co-based catalysts.[5] In an effort to understand this catalytic activation of methane by metal centers, fundamental aspects of such interactions have been studied by examining the gas-phase reactions between atomic metal cations and methane, as explored by several groups.[6-55] Bohme and co-workers surveyed the gas-phase reactions between atomic metal cations (s, p, d, and lanthanides) and methane at thermal energies using a selected-ion flow tube (SIFT) mass spectrometer.[40] The only atomic metal ions found to activate methane exothermically at room temperature were the third row transition metals, Ta^+, W^+, Os^+, Ir^+, and Pt^+, as determined previously by Irikura and Beauchamp,[16-17] along with As^+ and Nb^+. These reactions of the third-row transition metals have been studied in more detail in subsequent studies.[27, 33-35, 43] Although niobium cations have been observed to form $NbCH_2^+ + H_2$ at thermal energy,[13, 40] this has been shown to be an endothermic process with a low endothermicity.[26] More recently, the structures of species formed in the reactions of many transition metal ions with methane at thermal energies have been interrogated using infrared multiple photon dissociation (IRMPD) and electronic action spectroscopies.[48-53, 55-66] In most cases, the MCH_2^+ products formed are metal carbene (with early metals exhibiting agostic interactions), although a few cases have found a preference for the $HMCH^+$ structure.[48, 58]

Among the f-block metals, neither singly[40] nor doubly[39] charged lanthanide cations are found to activate methane at thermal energies, although both Ce^+ and Gd^+ formed a $Ln^+(CH_4)$ adduct. When Ce^+, Pr^+, Nd^+, and Sm^+ were produced using an inductively coupled plasma (ICP) source at an estimated temperature of 8000 K, these ions were observed to react exothermically at thermal energy with deuterated methane.[67] Experimental studies of actinide chemistry are particularly interesting because of the involvement of f-orbitals in bonding and their importance in the nuclear fuel cycle.[68] Despite the importance, experimental studies of actinides remain lightly

explored because most actinides are radioactive, with the least radioactive species being uranium and thorium. Theoretically, methane activation by actinide ions (Ac^+, Th^+, Pa^+, U^+, Np^+, and Pu^+) was studied by Almeida et al. using several density functional theory (DFT) levels.[69] They predicted that formation of an H-An^+-CH_3 intermediate is an exoergonic process except for Pu^+ and that Th^+ was the only actinide for which the process was barrierless (although the barrier for U^+ was low). These authors did not consider the complete reaction leading to dehydrogenation. Their findings were in agreement with experiments by Gibson et al., who found that among the actinide cations they studied (Th^+, Pa^+, U^+, Np^+, Pu^+, Am^+, and Cm^+), only Th^+ reacted with methane at thermal energies to dehydrogenate and form $ThCH_2^+$,[70] as observed previously by Marçalo et al.[71] In both experimental studies, the reaction rate was very slow, having efficiencies of 0.009 ± 0.005 and 0.02 ± 0.01, respectively. Subsequent guided ion beam tandem mass spectrometry (GIBMS) studies of this reaction demonstrated that the reaction exhibited a barrier,[45] thus explaining the low reaction efficiency at thermal energies. In that work, ThH^+, $ThCH_3^+$, and $ThCH^+$ products formed in endothermic reactions were identified as well, their thermochemistry characterized experimentally, and their structures explored theoretically. The theoretical results obtained paralleled those obtained earlier by Russo and co-workers,[72] although including spin-orbit effects was found to be critical to reproducing the experimental observations.[45] The dications of both Th and U have also been observed to activate methane (forming $AnCH_2^{2+} + H_2$) at thermal energies.[73]

Interestingly, among all of these gas-phase methane activation studies, the earliest was that of Armentrout and Beauchamp, who used an ion beam experiment to study the $U^+ + CD_4$ reaction over a wide range of energies.[6, 74] The only product they observed was $UD^+ + CD_3$, which was analyzed to reveal a U^+-H bond dissociation energy (BDE) of 2.9 ± 0.2 eV. The potential energy surfaces for the reaction of methane with U^+ have been explored previously using PW91/ZORA and B3LYP/SDD levels of theory by Russo and co-workers.[72] They predicted that formation of the H-U^+-CH_3 intermediate was exothermic, but inhibited by a barrier corresponding to the oxidative addition transition state. Further, they predicted that dehydrogenation to yield UCH_2^+ +

H_2 was an endothermic process that could retain quartet spin throughout.[45] Very recently, an inductively-coupled plasma tandem mass spectrometer (ICP-MS/MS) has been used to examine the kinetic energy dependence of the reaction of An^+ = Th^+ - Am^+ with perdeuterated methane.[75] Here, endothermic reactions yielded AnD^+, AnC^+, $AnCD^+$, $AnCD_2^+$, and $AnCD_3^+$ products for Th^+, Pa^+, U^+, and Np^+, whereas Pu^+ yielded only PuD^+ and $PuCD_2^+$ and Am^+ formed only AmD^+. By estimating the temperature of the ICP ion source, thresholds for these species were determined and converted to BDEs for all products.

In the present work, we reexamine the reaction of atomic uranium cations with methane and methane-d4 using GIBMS. The work includes measurement of the absolute experimental cross sections for several ionic products, UH^+, UC^+, UCH^+, UCH_2^+, and UCH_3^+ (along with their perdeutero analogues). Because all these products are formed in endothermic reactions, an analysis of the kinetic energy dependence of these reactions enables us to experimentally determine BDEs for all five product ions with precision. We supplement this experimental work with quantum chemical calculations that are used to compare to the experimental BDEs and those of Bubas et al.[75] Theoretical calculations are also used here to elucidate the reaction pathways for all products.

Methods

Experimental. The GIBMS instrument used in this work has been described in detail earlier.[76-77] The reactant U^+ cation was generated using a direct current discharge/flow tube (DC/FT) source with depleted uranium metal as the cathode held at -1.5 kV.[78] Ar carrier gas flowed over the cathode and was ionized by the electric field, such that these ions collided with the cathode, sputtering uranium cations and atomic uranium that could be ionized by secondary ionization processes such as electron ionization and Penning ionization in the Ar plasma cloud.[79] These ions are thermalized in the meter-long flow tube by ~10^5 collisions with the Ar carrier gas. In previous work, this DC/FT source produced atomic metal ions having an effective electronic temperature of 700 ± 400 K when operated with a 10% Ar, 90% He mixture.[80-86] Because of current He shortages, we used 100% Ar in the current work, however we presume a similar distribution of

electronic states was created. The ground state of U^+ is a $^4I_{9/2}$ ($5f^37s^2$) term with a low-lying $^6L_{11/2}$ ($5f^36d^17s^1$) term at 0.036 eV. At 300 K, these levels are populated as 76% and 23%, respectively, changing to 43% and 35%, respectively, at 1100 K with additional contributions of 13%, 6%, and 3% in excited states ($^6K_{9/2}$,$5f^36d7s$), ($^6L_{13/2}$,$5f^36d7s$), and ($^6K_{11/2}$,$5f^36d7s$) at 0.113, 0.217, and 0.285 eV, respectively.[87-88] At a conservative temperature of 700 ± 400 K, the U^+ reactant has an average electronic energy, E_{el}, of 0.03 ± 0.02 eV.[89] Notably, this DC/FT ion source produces atomic uranium cations with a much better controlled electronic and translational state distribution compared to the surface ionization source used by Armentrout and Beauchamp[6] and to the ICP source used by Bubas et al.[75] The consequences of this are discussed below.

These ions were extracted and focused through a magnetic momentum analyzer that selected the parent $^{238}U^+$ cation. Ions exiting the analyzer were decelerated to a well-defined kinetic energy and focused into a radiofrequency (rf) octopole ion beam guide that radially trapped the ions.[76, 90-91] A portion of the octopole passed through a static reaction cell containing the neutral reactant gas (CH_4 or CD_4) at ~0.4, 0.6, and 1.2 mTorr pressure. Such low pressures of the neutral reactants ensured that more than one collision between reactants had a very low probability. Indeed, the cross sections for all products exhibited no dependence on methane pressure, indicating that single collision conditions prevailed. Reactant and product ions drifted to the end of the octopole, where they were extracted and focused into a quadrupole mass filter for mass analysis. Ion intensities were measured using a Daly-type detector[92] operated in a pulse counting mode. Laboratory ion energies (E_{lab}) were converted to the center-of-mass (E_{CM}) frame using the equation, $E_{CM} = E_{lab} \times m/(m + M)$, where m and M correspond to the mass of neutral and ionic reactants, respectively. The absolute zero of kinetic energy and full width at half-maximum (FWHM) of the ion kinetic energy distribution were determined by using the octopole guide as a retarding potential analyzer.[76] Ion energies in these experiments have a distribution that is close to Gaussian with a FWHM that lies in the range of 0.4 - 0.6 eV in the lab frame. All experimental energies reported in this paper are in the center-of-mass frame. In addition, the intensities of the reactant and product ions are converted to absolute reaction cross sections using a Beer's law-like

formula after correcting for background signal obtained with no gas in the collision cell, as described in detail elsewhere.[76]

At higher energies, product ions can undergo further dissociation or competition with other channels, such that their cross sections decline. As described previously,[93] this subsequent dissociation can be described using parameters p and E_D, where p is an adjustable parameter analogous to n and E_D is the experimental onset for the decline.

Data Analysis. The kinetic energy dependence of the cross sections for all endothermic reactions was modeled using equation 1.

$$\sigma(E) = \sigma_0 \sum g_i (E + E_{el} + E_i - E_0)^n / E \qquad (1)$$

Here, σ_0 is an energy-independent scaling factor; E is the relative (CM) kinetic energy of the reactants; E_{el} is the average electronic energy of the U^+ reactant (defined above); E_i represents the internal energy of the neutral reactant's electronic, rotational, and vibrational states having populations g_i ($\sum g_i = 1$); n represents an adjustable parameter that controls the shape of the cross section; and E_0 is the reaction threshold at 0 K. Eq 1 was convoluted over the kinetic energy distributions of the reactants before comparison with the experimental spectrum. The parameters σ_0, n, and E_0 were then optimized using a nonlinear least-squares method to best reproduce the experimental cross section.

Computational. The Gaussian16 suite of programs was used for most quantum chemical calculations.[94] The basis set used for the U^+ cation was a correlation consistent polarized core valence (including core-valence correlation corrections) quadruple-ζ basis set, cc-pwCVQZ-PP (20s17p12d11f7g4h1i)/[9s9p8d8f7g4h1i] developed by Peterson, which uses a Stuttgart/Koeln fully relativistic small core (60 electrons) effective core potential (ECP60MDF pseudopotential).[95-96] The aug-cc-pCVXZ and aug-cc-pVXZ (X = T, Q) basis set was used for hydrogen and carbon atoms, respectively.[97] For calculations of the BDEs, the cc-pwCVXZ-PP/aug-cc-pCVXZ/aug-cc-pVXZ (X = T, Q) basis sets were used with UB3LYP and UCCSD(T)//UB3LYP levels of theory, where the U^+ (5s,5p) and the C (1s) orbitals were frozen for the electron correlation calculations. In the following, the unrestricted (U) designation is

dropped and this combination of basis sets will be referred to simply as VTZ and VQZ. Complete basis set (CBS) extrapolations for Hartree-Fock (HF) energies were performed using the Karton-Martin method described by equation 2, where X = 3 and 4 for TZ and QZ basis sets, respectively.[95, 98]

$$E_X = E_{CBS} + A(X+1)e^{-6.57\sqrt{X}} \quad (2)$$

Equation 3 describes the CBS extrapolation for the correlation energy in CCSD(T) calculations.[95, 99-100]

$$E_X = E_{CBS} + B(X+1/2)^{-4} \quad (3)$$

Relaxed potential energy surface (PES) scans were done at the B3LYP/VTZ level of theory in order to locate transition states. CBS extrapolations were again performed to determine the energies for all stationary states located along the PES using both B3LYP and CCSD(T)//B3LYP single point energies. Notably, the B3LYP/CBS and CCSD(T)/CBS approaches yield BDEs for the CH_x and H_2 species that match experimental values within 0.07 and 0.03 eV, respectively, with average absolute deviations of 0.039 and 0.016 eV, respectively (see Table S1).

Spin-orbit energy correction estimates were obtained using complete active space SCF (CASSCF)[101] followed by second order multiconfigurational perturbation theory (CASPT2)[102] to estimate dynamical correlation effects and subsequent restricted active space state interaction (RASSI)[103] to compute the spin-orbit eigenstates. This approach was utilized in earlier work on the BDE of UH^+ [89] and is similar to the methods used by Bross and Peterson, Antonov and Heaven, and Dolg and Cao for estimating the role of spin-orbit on the spectra of UF^+, UCl^+, and the spectra and BDE of UH.[104-106] The relativistic Atomic Natural Orbital (ANO-RCC-VQZP) basis sets available in OpenMolcas and the relativistic DK2 Hamiltonian were used to compute the scalar relativistic and spin-orbit coupling effects. State-averaged CASSCF and CASPT2 were used to generate the lowest 16 states for UCH_x^+ in each irrep of the C_s point group with spin states 5, 3, 1 (x = 1,3) and 6, 4, 2 (x = 2) using an active space consisting of the uranium 5f, 6d, and 7s orbitals and carbon 2p orbitals. In the subsequent CASPT2 calculations, the U(6s), U(6p), and the C(2s) orbitals were also correlated. The default OpenMolcas IPEA

shift of 0.25 and imaginary shift of 0.1 were used in the CASPT2 calculations, with the multi-state optimization turned off. All generated states were included in the RASSI calculations to generate the spin-free and spin-orbit states. The ground state was used for the calculation of the BDE.

Results and Discussion

Experimental results

The reaction between the atomic uranium cation and methane (methane-d_4) results in reactions (4) – (8).

$$U^+ + CH_4\ (CD_4) \rightarrow UCH_3^+ + H\ (UCD_3^+ + D) \quad (4)$$

$$\rightarrow UCH_2^+ + H_2\ (UCD_2^+ + D_2) \quad (5)$$

$$\rightarrow UCH^+ + H_2 + H\ (UCD^+ + D_2 + D) \quad (6)$$

$$\rightarrow UC^+ + 2\ H_2\ (UC^+ + 2\ D_2) \quad (7)$$

$$\rightarrow UH^+ + CH_3\ (UD^+ + CD_3) \quad (8)$$

The experimental cross sections for these reactions are shown in Figures 1 and 2. The use of the perdeuterated reactant reduced the mass overlap between the UCH_x^+ (UCD_x^+) products and between the U^+ and the UH^+ (UD^+) product and also permits study of possible isotopic effects on the reaction pathway. Mass overlap of the dominant UCH_2^+ (UCD_2^+) product with the UCH_3^+ (UCD_3^+) and UCH^+ (UCD^+) products at low energy was obvious and was subtracted to yield the results shown in both figures. Likewise, signals obtained at the mass of UC^+ were corrected for mass overlap with the UCH^+ (UCD^+) product.

It can be seen in both figures that all products resulting from these reactions were formed by endothermic reaction pathways. At low energy, the dehydrogenated product, UCH_2^+ (UCD_2^+), dominates until the uranium hydride cation, UH^+ (UD^+), and UCH_3^+ (UCD_3^+) start forming. The UCH_2^+ (UCD_2^+) cross sections begin to decline where these latter products start to be formed, and the total cross section changes smoothly with energy, which indicates that they all share a common intermediate. The observation that the UH^+ (UD^+) and UCH_3^+ (UCD_3^+) products have similar

thresholds suggests that the U^+-H (U^+-D) BDEs are comparable to the U^+-CH_3 (U^+-CD_3) BDEs, consistent with a uranium methyl structure. Even though the energetics of reactions (4) and (8) are similar, the UH^+ (UD^+) product dominates in magnitude because of angular momentum constraints, as discussed in detail previously.[10, 21, 34, 107] Briefly, because the reduced mass of the reaction (8) products, 14.1 (16.7) Da, is so much larger than that for the reaction (4) products, 1.0 (2.0) Da, and comparable to that of the reactants, 15.0 (18.4) Da, angular momentum is conserved for a much broader range of impact parameters for the formation of the UH^+ (UD^+) products than for UCH_3^+ (UCD_3^+).

It can also be seen that the UCH_3^+ (UCD_3^+) cross section declines at higher energies, just as the UCH^+ (UCD^+) cross section begins. This indicates that the UCH_3^+ (UCD_3^+) product undergoes dehydrogenation to form UCH^+ (UCD^+). It is also possible that the UCH_3^+ (UCD_3^+) product could dissociate by H (D) atom loss, yielding UCH_2^+ (UCD_2^+), although there is no obvious feature at high energies in the cross sections of the latter products that would suggest this process is efficient. Rather, the sum of the UCH_3^+ (UCD_3^+) and UCH^+ (UCD^+) cross sections declines starting near D_0(H-CH_3) = 4.48 eV,[108] indicating that UCH_3^+ (UCD_3^+) does dissociate to U^+ + CH_3 (CD_3). The UH^+ (UD^+) products do not exhibit a similar decline because much of the excess energy can be carried away by the CH_3 (CD_3) neutral product, unlike the H (D) neutral products, which have no internal degrees of freedom.

Figure 2 also includes the UD^+ + CD_3 cross section measured by Armentrout and Beauchamp using an ion beam apparatus without an octopole ion guide.[6] It can be seen that the shape of the cross section is similar, although the absolute magnitude measured here is about three times larger. This difference can be attributed to the reduced collection efficiency of this more primitive instrument. Also, note that the previous UD^+ cross section tails to lower energies, which is a result of forming U^+ using a surface ionization source operated at an estimated temperature of 2300 K. This occupies many excited electronic states such that the average electronic energy is 0.19 eV, with states up to 0.7 eV having populations above 1%.

Thermochemical Analysis: All cross sections have been modeled using Eq. (1), with optimized fitting parameters provided in Table 1. These models are shown in both Figures 1 and 2 and can be seen to reproduce the data with fidelity over wide energy and magnitude ranges. Because this modeling takes into account the internal and kinetic energy distributions of both reactants, E_0 values obtained correspond to thresholds at 0 K.

UH^+: The threshold for UH^+ formation obtained experimentally was 2.11 ± 0.15 eV. Given the 0 K BDE of H-CH_3, 4.482 ± 0.001 eV,[108] D_0 (U^+-H) = D_0(H-CH_3) - E_0 is found to be 2.37 ± 0.15 eV. This value is in good agreement with a recent study of U^+ reacting with H_2, HD, and D_2 in our lab,[89] which reported a final value for D_0(U^+-H) of 2.48 ± 0.06 eV, taken from the average results for reactions with all three reactants. The threshold for UD^+ in reaction (8) (2.10 ± 0.13 eV, Table 1) is very similar to that for UH^+ formation and, combined with D_0 (D-CD_3) = 4.58 ± 0.01 eV,[27] results in D_0 (UD^+) = 2.48 ± 0.13 eV. A calculated zero point energy correction of 0.029 eV[89] then leads to D_0 (UH^+) = 2.45 ± 0.13 eV, in excellent agreement with the previous value. A weighted average of the two values determined here is 2.42 ± 0.10 eV, again in good agreement with the previous value, which we believe remains our best experimental determination. This value can also be converted to the proton affinity (PA) of the uranium atom by combining it with the ionization energies (IE) of H, 13.5984 eV, and U, 6.19405 eV,[109] in the formula PA(U) = D^0 (UH^+) + IE (H) – IE (U) = 9.88 ± 0.06 eV.

UC^+: UC^+ (UC^+) formation results from dehydrogenation of the UCH_2^+ (UCD_2^+) product, reaction (7). In order to account for the fact that the cross sections for the UCH_2^+ (UCD_2^+) precursor are declining at the energies where UC^+ is formed, we analyzed the UC^+ cross sections using Eq. (1) after dividing by the UCH_2^+ (UCD_2^+) cross section. This procedure led to the parameters listed in Table 1. Given D_0 (C-$2H_2$) = 8.063 ± 0.001 eV,[108] the threshold for UC^+ + 2 H_2 formation of 4.12 ± 0.10 eV leads to D_0 (U^+-C) = 3.94 ± 0.10 eV. Similar calculations for the deuterated counterpart, with D_0 (C-$2D_2$) = 8.21 ± 0.03 eV and E_0(UC^+) = 4.26 ± 0.12 eV, lead to D_0 (U^+-C) = 3.95 ± 0.12 eV. Because the mass overlap corrections are much smaller for the CD_4 system, we take the latter value as our best experimental determination here. Both values are within

experimental uncertainty of a study reacting U^+ with CO in our lab,[110] which reported a final value for $D_0(U^+\text{-}C)$ of 4.03 ± 0.13 eV after correcting for competition with the dominant UO^+ channel using a phase space model. A weighted average of these two independent values is 3.99 ± 0.09 eV.

UCH^+: UCH^+ (UCD^+) formation results from dehydrogenation of the UCH_3^+ (UCD_3^+) product. Given D_0 (H-CH_3) = 4.482 eV and D_0 (H_2-CH) = 4.591 ± 0.001 eV,[108] the threshold for $UCH^+ + H + H_2$ formation of 4.32 ± 0.16 eV leads to D_0 (U^+-CH) = 4.75 ± 0.16 eV. Similar calculations for the deuterated counterpart, with D_0 (D-CD_3) = 4.58 eV, D_0 (D_2-CD) = 4.67 ± 0.02 eV,[27] and E_0 (UCD^+) = 4.26 ± 0.10 eV, lead to a bond dissociation energy of 4.99 ± 0.10 eV. The expected zero-point energy correction is 0.015 eV, calculated using the theoretical vibrational frequencies discussed below, such that the latter BDE is equivalent to D_0 (U^+-CH) = 4.97 ± 0.10 eV. A weighted average of these two values leads to D_0 (U^+-CH) = 4.91 ± 0.09 eV.

UCH_2^+: This product is formed by the dehydrogenation of methane in reaction (5). Here, we presume that the observed threshold corresponds to the energy of the product asymptote rather than a barrier along the potential energy surface, which can be verified by the calculations below. Given the experimental threshold for this reaction with CH_4 of 0.63 ± 0.05 eV along with D_0 (H_2-CH_2) = 4.743 ± 0.001 eV,[108] we find the 0 K BDE for UCH_2^+ to be 4.11 ± 0.05 eV. For the perdeuterated system, a similar threshold energy (0.68 ± 0.06 eV) and D_0 (D_2-CD_2) = 4.82 ± 0.03 eV[27] leads to D_0 (U^+-CD_2) = 4.14 ± 0.07 eV. The zero-point energy difference calculated here is 0.02 eV, such that the latter value converts to D_0 (U^+-CH_2) = 4.12 ± 0.06 eV. The two values lead to a weighted average of 4.11 ± 0.04 eV.

UCH_3^+: The thresholds for reaction (4) with CH_4 (CD_4) are 2.11 ± 0.12 (2.09 ± 0.15) eV and lead to 0 K BDEs for U^+-CH_3 (U^+-CD_3) of 2.37 ± 0.12 (2.49 ± 0.15) eV. The calculated zero-point energy difference is 0.012 eV, such that the results for UCD_3^+ convert to D_0 (U^+-CH_3) = 2.48 ± 0.15 eV. A weighted average of these two values yields D_0 (U^+-CH_3) = 2.41 ± 0.09 eV. The similarity between this value and that for D_0 (U^+-H) = 2.42 ± 0.10 eV determined here suggests that the UCH_3^+ species has a single covalent bond between uranium and the ligand, indicating a uranium methyl structure. This structure was confirmed by the computations described below.

Similar to the proton affinity, the methyl cation affinity of atomic uranium can be derived from this BDE using IE (CH_3), 9.843 ± 0.002 eV,[111] yielding 6.06 ± 0.09 eV.

UCH_{x-1}^+-H bond energies. Given the experimental values of $D_0(U^+\text{-}CH_x)$ above, one can also combine these to determine the sequential bond energies for removing a hydrogen atom. This calculation requires the CH_2-H, CH-H, and CH bond energies as well (4.738, 4.332, and 3.466 eV, all ± 0.001 eV).[108] The derived BDEs for x = 3, 2, and 1 are 3.04 ± 0.10, 3.53 ± 0.10, and 4.39 ± 0.13 eV, respectively. The first two values are weaker than typical CH BDEs because a π bond between U^+ and C is formed upon loss of the hydrogen atom. Because UCH^+ and UC^+ have similar bond orders, the UC^+-H BDE is more typical of a CH bond energy.

Theoretical results: The ground state of uranium cation has been experimentally found to be ^{4}I ([Rn]$5f^37s^2$) with other low-lying states being ^{6}H ($5f^37s^2$), ^{6}I ($5f^37s^2$), ^{6}K ($5f^37s^2$), ^{6}L ($5f^37s^2$), and ^{6}M ($5f^37s^2$).[87-88] This ground state was successfully located by Russo and co-workers using the B3LYP/SDD level of theory[72] and in previous work from our lab using the cc-pwCVQZ-MDF basis set with CCSD(T), B3LYP, M06, and PBE0 levels of theory.[89] There it was found that the experimental excitation energies of electronic states of U^+ were reproduced best by B3LYP and CCSD(T) when the 5s and 5p electrons on U were frozen. Therefore, these levels of theory were utilized for all further calculations performed here. In all cases, the results correspond to the use of the cc-pwCVQZ-PP/aug-cc-pCVXZ/aug-cc-pVQZ (VQZ) basis set unless a CBS extrapolation is specified.

UH^+: In agreement with previous theoretical work in our laboratory,[89] UH^+ was predicted to have a ^{5}I ($1\sigma^2 2\sigma[\pi\delta\varphi]$) ground state with a bond length of 1.973 Å at the B3LYP/VQZ level of theory. Here, the 1σ is the bonding molecular orbital (MO), 2σ is largely a 7s nonbonding orbital, and the square brackets indicate 5f nonbonding MOs on U. Previous work also explored different possible states of UH^+, finding that a $^5\Phi$ ($1\sigma^2 2\sigma[\pi^2\varphi]$) state was very similar in energy.

UC^+: Previous theoretical work in our laboratory[110] predicted that after spin-orbit corrections, UC^+ has a $^4H_{3.5}$ ($1\sigma^1 1\pi^4[\delta\varphi]$) ground state with a bond length of 1.834 Å at the

B3LYP/VQZ level of theory. Both the 1σ and 1π orbitals are bonding MOs. The previous work also explored different possible states of UC^+, finding ten states within 1 eV of the ground state. Without spin-orbit corrections, a $^4\Sigma^-$ ($1\sigma^1 1\pi^4[\delta^2/\varphi^2]$) state was calculated to be the ground state.

UCH^+: UCH^+ was predicted to have a $^3\Sigma^+$ ground state with a linear structure at the B3LYP/VQZ level of theory. This species has a U-C bond distance of 1.876 Å and a CH bond distance of 1.088 Å. Vibrational frequencies (unscaled) include 591 (degenerate bend), 868 (UC stretch), and 3135 (CH stretch) cm^{-1}. The electronic structure shows a triple bond between U and C with two non-bonding electrons in the two 5fφ-like MOs. At the B3LYP/VTZ level, we also located the HUC^+ ($^3A''$) isomer, finding it lies 2.02 eV above UCH^+, Table S2 of the Supporting Information.

UCH_2^+: The calculated ground state of UCH_2^+ is $^4A''$ with a planar metal carbene geometry that has an agostic structure where one H is tilted toward the metal, which allows donation of electron density from a CH bond into an empty d orbital on the metal. This agostic structure is characteristic of the carbenes of early transition metal cations[34, 37, 49, 58] and also $ThCH_2^+$.[45] Geometrical parameters predicted here (UC bond distance of 2.042 Å, CH bond distances of 1.086 and 1.128 Å, and ∠UCH bond angles of 87.8° and 162.1°) are similar to the structures reported by Russo and co-workers,[72] who also predicted a $^4A''$ ground state. This molecule has a UC double bond with the three unpaired electrons residing in three 5f MOs (essentially $\sigma\varphi^2$, ignoring the distortions intrinsic to Cs symmetry).

The CH_2 wagging motion passes through the symmetric $^4A_2$ state (a transition state having C_{2v} symmetry and an imaginary frequency of 394 cm^{-1}) lying only 0.10 eV higher in energy. A $^4A'$ excited state was predicted to lie 0.36 eV higher in energy, where one of the π-bonding electrons is moved to a 7s-like a′-orbital on uranium.

To ensure that the structure of the UCH_2^+ product ion was appropriately characterized, we examined alternative structures including $HUCH^+$ ($^2A''$), $(H_2)UC^+$ ($^4A''$), $(H_2)UC^+$ ($^2A''$), and $(H)_2UC^+$ ($^2A_1$) at the B3LYP/VTZ level of theory. As reported in Table S2 of the Supporting

Information, these lie 1.56, 2.92, 3.06, and 4.28 eV, respectively, above the uranium carbene cation.

UCH_3^+: UCH_3^+ has a $^5A_1$ ground state (C_{3v} symmetry) with a $1\sigma^2 2\sigma[\pi\delta\varphi]$ electronic configuration, where the 1σ electrons are the single U-C covalent bond, the 2σ is largely a 7s nonbonding MO, and the other three electrons are in 5f nonbonding MOs on U. The UC bond length is 2.309 Å, the CH bonds are uniformly 1.099 Å long, and ∠UCH bond angles are 111.2°.

The uranium methyl cation structural preference was investigated computationally. Alternative structures to UCH_3^+ including $HUCH_2^+$ ($^3A''$), $(H_2)UCH^+$ (collapses to $HUCH_2^+$, $^3A''$), $(H)_2UCH^+$ ($^3A_2$), $(H)_2UCH^+$ (^1A), $(H_2)HUC^+$ ($^3A''$), $(H_2)HUC^+$ (^1A), and $(H)_3UC^+$ (collapses to $(H_2)HUC^+$, ^1A) were calculated and compared energetically at the B3LYP/VTZ level of theory. These alternative structures were predicted to lie significantly higher in energy compared to UCH_3^+, by 1.33, 3.83, 3.86, 4.46, and 4.64 eV, respectively, Table S2.

Spin-orbit corrections: Spin-orbit (SO) corrections are required to provide the most accurate comparison between experimental and theoretical BDEs because the experimental values at 0 K correspond to the lowest level of the molecular state, as well as that of the dissociation products. In contrast, our theoretical values were determined for the average of all SO states of reactants and products.

UH^+: In a recent paper,[89] SO corrections for UH^+ were discussed in detail. The SO corrections were calculated at the CASSCF-CASPT-RASSI level of theory for UH^+ (^5I) and U^+ (^4I), yielding values of 0.779 and 0.852 eV. The latter value is in good agreement with the difference between the energy of the $^4I_{9/2}$ ground level and the experimental average of all SO levels of the ^4I manifold, 0.849 eV.[87-88] Thus, it was established that the theoretical BDEs of UH^+ should be decreased by 0.074 eV to account for SO effects.

UC^+: As detailed elsewhere,[110] the ground state of UC^+ is $^4H_{3.5}$ with a SO correction to the calculated BDE of -0.20 eV.

UCH^+: The ground state of UCH^+ is $^3\Sigma^+$, which has no orbital angular momentum. Therefore, it might be imagined that there is no SO correction for this molecule; however, because there are two 5f-electrons, the SO correction for UCH^+ is non-zero. Here, we calculate that the overall SO correction to $D_0(U^+\text{-}CH)$ should be -0.180 eV.

UCH_2^+: Again, because the ground state of UCH_2^+ is $^4A''$, which has no orbital angular momentum, it might be imagined that there is no SO correction for this molecule; however, because there are three 5f-electrons, the SO correction for UCH_2^+ is also non-zero. Here, we calculate that the overall SO correction to $D_0(U^+\text{-}CH_2)$ should be -0.308 eV.

UCH_3^+: For this molecule, there are three unpaired 5f-electrons, which again leads to an appreciable SO correction for the UCH_3^+ BDE. Here, we calculate that the overall SO correction to $D_0(U^+\text{-}CH_3)$ should be -0.158 eV.

Theoretical thermochemistry: We have calculated the BDE of each product using CCSD(T)/CBS//B3LYP/VQZ and B3LYP/CBS levels of theory. Table 2 compares these theoretical BDEs with those found experimentally. CCSD(T) and B3LYP levels give values of 2.48 and 2.61 eV for the U^+-H BDE, respectively, changing to 2.41 and 2.53 eV, respectively, after including SO corrections for UH^+ and U^+. Both values are comparable to the weighted average of experimental values obtained in a previous experimental study of U^+ reacting with H_2, HD, and D_2 in our lab, 2.48 ± 0.06 eV. More advanced methods (CCSD(T)/CBS with CASPT2 and Feller-Peterson-Dixon, FPD, method[112]) have also predicted a value of 2.44 ± 0.05 eV,[113] similar to our CCSD(T)/CBS value.

For UC^+, complete basis set extrapolations of previously calculated BDEs at the CCSD(T) and B3LYP levels[110] give values of 4.02 and 3.82 eV, respectively, changing to 3.82 and 3.62 eV, respectively, after including SO corrections for UC^+ and U^+. More advanced methods (FPD method) have also predicted a value of 4.10 eV,[114] similar to our CCSD(T)/CBS value. All these values are comparable to the experimental value obtained here, 3.95 ± 0.12 eV, and previously,[110] 4.03 ± 0.13 eV, and the weighted average of these independent values, 3.99 ± 0.09 eV.

The theoretical BDE for U^+-CH was calculated to be 4.90 and 4.51 eV at the CCSD(T)/CBS and B3LYP/CBS levels of theory, respectively. Applying the calculated SO correction of 0.180 eV lowers these values to 4.72 and 4.33 eV, respectively. The CCSD(T) result without SO corrections agree well with the experimental weighted average value of 4.91 ± 0.09 eV. Theoretical BDEs for U^+-CH_2 were predicted to be 3.98 and 3.81 eV at the CCSD(T)/CBS and B3LYP/CBS levels of theory, respectively, which drop to 3.67 and 3.50 eV, respectively, when the SO correction is applied. Again, the CCSD(T) result without SO corrections is in reasonable agreement with the experimental value, 4.11 ± 0.04 eV. The theoretical U^+-CH_3 BDEs of 2.72 and 2.67 eV, CCSD(T)/CBS and B3LYP/CBS, respectively, decrease to 2.56 and 2.51 eV after applying the calculated SO correction. These latter values are in reasonable agreement with the experimental value of 2.41 ± 0.09 eV.

Overall, a comparison of these BDEs along with those calculated for UC^+ reveals that the CCSD(T)/CBS values reproduce experiment better than the B3LYP/CBS values and that including the SO corrections makes the agreement with experiment slightly worse. Mean absolute deviations between experiment and theory for the five species in Table 2 are 0.26 ± 0.10 (0.35 ± 0.26) eV for B3LYP/CBS without (with) SO corrections and 0.10 ± 0.13 (0.20 ± 0.15) eV for CCSD(T)/CBS results. Given that the average experimental uncertainty (1 standard deviation) is 0.08 eV, the CCSD(T) results reproduce the experimental values well.

Figure 3 shows the bond energy-bond order (BEBO) plot for An^+-L species, where An = U and Th, and L = H and CH_x (x = 1 – 3). Thermodynamic values for D_0 (Th^+-L) are taken from references [45] and [115]. In this plot, D_0 (An^+-L) has been plotted versus D_0 (L-L) taken from reference [108]. BEBO plots have been previously used to experimentally determine the bond order of many transition metal and actinide systems.[27, 29, 34, 37, 43] This plot demonstrates that the bond order of UH^+ and U^+-CH_3, U^+=CH_2, and U^+≡CH increases from 1 to 2 to 3, as anticipated and verified by theory. The relative slopes for the two actinides indicate that Th has stronger bonds by 17%. This can be attributed, at least in part, to the fact that the J = 3/2 ground level of Th^+ has a mixture of $6d7s^2$ and $6d^27s$ configurations, whereas U^+ has a doubly occupied 7s orbital in its $5f^37s^2$ ground

configuration. Thus, U^+ must be promoted to a configuration suitable for forming covalent bonds, whereas the $6d^27s$ configuration is already appropriate. The costs of this promotion energy will lower the adiabatic BDEs of the uranium species.

A Natural Bond Orbital (NBO) analysis[116-117] computed at the UB3LYP/VQZ level of theory confirms the BEBO analysis, Table S3. UCH^+ is shown to form a triple bond (bond order =3) with one σ bond and two π bonds, UCH_2^+ forms a double bond with one σ and one π bond, and UCH_3^+ and UH^+ have a single σ bond. For all three UCH_x^+ species, the σ bonds have contributions from 7s, 6d, and 5f orbitals on uranium and 2s and 2p orbitals on carbon, whereas the 1s orbital on H is involved for UH^+. The π bonds have contributions mostly from 6d and 5f orbitals on uranium and 2p orbitals on carbon. For all bonds, the U and C populations (%NBO) lean towards carbon with 68 – 82% character for the σ bonds and 55 – 75% character for the π bonds.

Table 2 also contains the BDEs obtained by Bubas et al. from their analysis of the kinetic energy dependence of the reactions of $U^+ + CD_4$, obtained using an ICP-MS/MS instrument.[75] The ICP source creates ions at a very high temperature, estimated in this study to be 6000 K. Using an assumed shift in the kinetic energy scale and this temperature, data similar to that shown here were analyzed using the same approach, Eq. (1), although the kinetic energy distributions of the ions and neutrals were not included in the analysis. It can be seen that the BDE obtained for UD^+ is comparable to that obtained here and previously. The BDE for UCH_2^+ is lower than the present value but just outside of their experimental uncertainty. BDEs for UCD^+ and UCD_3^+ are much larger than those found here, outside of their already generous uncertainties. This is also true of their value for UC^+ compared to the present work and a previous GIBMS study.[110] We believe that these differences can be attributed to errors in the absolute energy scale and the temperature of the ICP source, which should generate ions in excited electronic states. Unfortunately, such errors are likely to propagate to all the actinide (An) systems studied in this work. Relative trends observed are likely to be more robust although because the excitation energies of excited electronic states vary for each actinide, the trends may be influenced by this factor as well. Overall, it can be

concluded that better characterization of the ICP source (both for the kinetic energy scale and electronic excitation) is needed for more quantitative thermodynamic information.

Potential energy surface of the reaction: Russo and co-workers previously explored the potential energy surface (PES) for the reaction of U^+ with methane at the B3LYP/SDD level of theory.[72] (They also calculated energies at the PW91/ZORA level, but these do not agree well with the experiment and hence are not considered further here.) Their calculations included a detailed theoretical analysis using natural bond orbital, atoms in molecules, and the electron localization function for all intermediates and the dehydrogenation products. They also considered spin states of doublet, quartet, and sextet, showing that the doublet and sextet spin surfaces lie above the quartet surface throughout the reaction. Therefore, we performed geometry calculations only for the quartet surface at the B3LYP level using the VTZ basis sets. These results parallel the results of Russo and co-workers well as can be seen by the BDEs for UH^+, UCH_3^+, and UCH_2^+ in Table 2. The structures of all intermediates (INT) and transition states (TS) located here are shown in Figure 4 with B3LYP/CBS and CCSD(T)/CBS single point energies listed in Table 3 and shown in Figure 5. (Note that these energies do not include SO corrections.) The Supporting Information provides geometrical parameters for all intermediates and transition states (Table S4), total electronic energies of all species (CCSD(T) and B3LYP, Table S5), and cartesian coordinates of all species (CCSD(T) level).

The initial intermediate formed (INT1) is an adduct of the atomic uranium cation and methane, $U^+(CH_4)$. This species has near C_{3v} symmetry, with three U-H bond distances within 0.001 Å of one another and the other (directed away from U) being 0.009 Å shorter. We find that $U^+(CH_4)$ lies 28 (16) kJ/mol lower than the ground state of the reactants, U^+ (^{4}I) + CH_4 ($^1A_1$), at the CCSD(T)/CBS (B3LYP/CBS) levels of theory.[45] This intermediate then proceeds to activate the C-H bond by progressing through the first transition state (TS1/2), where one of the hydrogens on methane shifts toward the uranium center. TS1/2 leads to the insertion intermediate, $H\text{-}U^+\text{-}CH_3$ (INT2), which is the global minima of the PES lying well below the reactant energy. This

intermediate has UC and UH bond lengths of 2.329 and 2.009 Å, respectively, and a ∠HUC bond angle of 93.9°. The bond lengths can be compared to those of isolated UCH_3^+ (2.309 Å) and UH^+ (1.973 Å), which indicates that single covalent bonds are maintained in INT2. The angle indicates that 6d orbitals on U are involved in bonding to H and CH_3.

At higher collision energies, INT2 can dissociate by cleavage of either the U-H or U-C bond to directly form the UCH_3^+ + H or UH^+ + CH_3 products. Calculations indicate that both products have similar threshold energies, 169 (168) and 192 (174) kJ/mol, respectively (158 and 166 kJ/mol, respectively, as predicted by Russo and co-workers[72]). Our calculated SO corrections for these products increase these values to 184 (183) and 199 (181) kJ/mol. These values can be compared to the experimental thresholds of 204 ± 15 and 204 ± 12 kJ/mol, respectively (from Table 1).

Alternatively, at lower energies, INT2 can rearrange by another hydrogen atom transfer from carbon towards the uranium cation in a four-centered transition state, TS2/3. Here, the incipient H-H bond has a length of 0.883 Å. TS2/3 leads to the third intermediate in which molecular hydrogen is bound to the final uranium carbene cation, $(H_2)U^+{=}CH_2$ (INT3). Here, the H-H bond length is 0.825 Å, slightly larger than free H_2 (0.743 Å at this level of theory, compared to 0.741 Å found experimentally[118]). TS2/3 is only 3.0 kJ/mol higher in energy than INT3 once zero-point energies have been included (and lower at the B3LYP level, as also predicted by Russo and co-workers). Indeed, in B3LYP/cc-pVDZ calculations, this transition state could not be optimized but collapsed to INT2. From INT3, loss of molecular hydrogen requires only 31 (34) (32, Russo and co-workers) kJ/mol and leads to the final products, UCH_2^+ ($^4A''$) + H_2 ($^1\Sigma_g^+$). As also predicted by Russo and co-workers, the overall dehydrogenation reaction can proceed entirely along the quartet spin surface. This dehydrogenation is calculated to require 71 (83) (71, Russo and co-workers) kJ/mol compared to 61 ± 5 kJ/mol found here experimentally (Table 1). Spin-orbit corrections increase the theoretical asymptotic energies by another 30 kJ/mol.

At high energies, the UCH_3^+ product can undergo dehydrogenation, leading to the formation of the UCH^+ + H_2 + H product channel. We calculate that this product asymptote lies at

398 (435) kJ/mol (415 (452) kJ/mol after SO corrections), which is comparable to our measured threshold energy of 417 ± 15 kJ/mol (Table 1).

Although SO corrections were not calculated for the intermediates and transition states, because these corrections lie in the range of 0.07 – 0.31 eV for all products, we do not anticipate that the qualitative aspects of the PES shown here will change appreciably.

Comparisons with activation of methane by thorium cations: Experimentally, the atomic thorium cation reacts with methane to undergo dehydrogenation with a threshold of only 0.17 ± 0.02 eV.[45] Theory indicates that this threshold corresponds to the analogue of TS1/2 rather than the $ThCH_2^+ + H_2$ product asymptote, which is calculated to lie below the energy of the reactants.[45] In contrast, the formation of $UCH_2^+ + H_2$ is limited by the product asymptote according to both the B3LYP/CBS and CCSD(T)/CBS levels of theory employed here (Figure 5) and B3LYP/SDD results of Russo and co-workers.[72] At higher energies, both Th^+ and U^+ exhibit formation of $AnH^+ + CH_3$, which clearly competes with the dehydrogenation process, as well as $AnCH_3^+ + H$, which has a similar threshold. The latter product decomposes at still higher energies by dehydrogenation to form $AnCH^+ + H_2$.

The bond energy of $ThCH_2^+$, >4.54 ± 0.09 eV, is substantially greater than that measured here for UCH_2^+, 4.11 ± 0.04 eV. CCSD(T) calculations suggest the former is 4.74 – 4.94 eV. This appreciable difference can be attributed to the difference in promotion energies needed to put the actinide cation into a configuration suitable for making a σ and π bond with CH_2. For Th^+, the J = 3/2 level is a mixture of $^2D(6d^17s^2)$ and $^4F(6d^27s^1)$, where the latter needs no promotion to form the double bond. In contrast, $U^+(^4I, 5f^37s^2)$ needs to promote both 7s valence electrons to 6d orbitals in order to form the double bond in UCH_2^+ ($^4A''$). Spectroscopic work indicates this promotion energy is 0.57 eV,[88, 119] accounting for most of the difference between the two An^+-CH_2 bond energies.

Conclusions

GIBMS experiments reveal that the reaction of methane with the atomic uranium cation produces five different products (UC^+, UCH^+, UCH_2^+, UCH_3^+, and UH^+) via endothermic reaction pathways. The dehydrogenation product ion (UCH_2^+) dominates the low-energy region, whereas the UH^+ product becomes dominant in the high-energy region. All products form through the insertion intermediate H-U^+-CH_3 (INT2). UCH_3^+ and UH^+ have very similar energy thresholds and can be formed directly from the H-U^+-CH_3 intermediate, whereas the formation of UCH_2^+ requires passing through the four-center TS2/3 as it loses molecular hydrogen. Because this latter channel is entropically less favorable than the simple bond cleavages leading to the UH^+ and UCH_3^+ products, its cross section declines as the latter products begin to be formed. UH^+ has a much larger reaction cross section than UCH_3^+ because of angular momentum constraints. At high energies, UCH_3^+ decomposes further by dehydrogenation, yielding the UCH^+ product.

Analyses of the kinetic energy dependent cross sections for all five products allow the thresholds for reaction to be determined. In combination with neutral thermochemistry, BDEs for uranium cations bound to H, C, CH, CH_2, and CH_3 were measured. The BDEs for UH^+ and UC^+ determined here agree well with previous measurements conducted in our laboratory.[89, 110] UCH_3^+ is found to have a similar BDE as UH^+, indicating that it has a methyl ligand, in agreement with calculations on this species and a simple BEBO analysis. The latter also shows that UCH_2^+ has a double bond, whereas UCH^+ has a triple bond, both in agreement with our theoretical analysis. Spin-orbit corrections are relatively small and do not greatly affect a favorable comparison between experimental and theoretical thermochemistry for the UCH_x^+ species.

The calculated potential energy surface for this reaction, which agrees well with results of Russo and co-workers, [72] is consistent with all products passing through a common intermediate, H-U^+-CH_3 (INT2) At low collision energies, this species decomposes by transferring another H-atom to the uranium center where it couples with the first hydride ligand to form H_2, which is readily lost to form UCH_2^+. At higher energies, this intermediate more readily cleaves either the UC or UH bonds to yield $UH^+ + CH_3$ or $UCH_3^+ + H$.

Acknowledgements

This work is supported by the Heavy Element Chemistry Program, Office of Basic Energy Sciences, U. S. Department of Energy, through Grant No. DE-SC0012249 (PBA). The authors also thank the Center for High Performance Computing at the University of Utah for the generous allocation of computer time. This research also used resources of the Bridge Xsede Computing Facility, which is a DOE Office of Science User Facility supported under Contract DE-AC05-00OR22725. An award of computer time was provided by the Innovative and Novel Computational Impact on Theory and Experiment (INCITE) program.

Supplemental Information. Table of experimental and computed bond dissociation energies for neutral reactants and products. Table of computed relative energies of all UCH_x^+ (x = 1 – 3) products. Tables of computed energies and geometries for species along the potential energy surface of Figure 5.

Author Declaration. The authors have no conflicts to disclose.

References

1. Haggin, J., Chemists Seek Greater Recognition for Catalysis. *Chemical & Engineering News Archive* **1993,** *71* (22), 23-27.
2. Arakawa, H.; Aresta, M.; Armor, J. N.; Barteau, M. A.; Beckman, E. J.; Bell, A. T.; Bercaw, J. E.; Creutz, C.; Dinjus, E.; Dixon, D. A.; Domen, K.; DuBois, D. L.; Eckert, J.; Fujita, E.; Gibson, D. H.; Goddard, W. A.; Goodman, D. W.; Keller, J.; Kubas, G. J.; Kung, H. H.; Lyons, J. E.; Manzer, L. E.; Marks, T. J.; Morokuma, K.; Nicholas, K. M.; Periana, R.; Que, L.; Rostrup-Nielson, J.; Sachtler, W. M. H.; Schmidt, L. D.; Sen, A.; Somorjai, G. A.; Stair, P. C.; Stults, B. R.; Tumas, W., Catalysis Research of Relevance to Carbon Management: Progress, Challenges, and Opportunities. *Chem. Rev.* **2001,** *101* (4), 953-996.
3. Crabtree, R. H., Alkane C–H activation and functionalization with homogeneous transition metal catalysts: a century of progress—a new millennium in prospect. *J. Chem. Soc. Dalton Trans.* **2001,** (17), 2437-2450.
4. Crabtree, R. H., Organometallic alkane CH activation. *J. Organomet. Chem.* **2004,** *689* (24), 4083-4091.
5. Lee, Y. J.; Hong, S. I.; Moon, D. J., Studies on the Steam and CO_2 Reforming of Methane for GTL-FPSO Applications. *Catal. Today* **2011,** *174*, 31−36.

6. Armentrout, P. B.; Hodges, R. V.; Beauchamp, J. L., Endothermic Reactions of Uranium Ions with N_2, D_2 and CD_4. *J. Chem. Phys.* **1977,** *66*, 4683-4688.
7. Halle, L. F.; Armentrout, P. B.; Beauchamp, J. L., Formation of Chromium Carbene Ions by Reaction of Electronically Excited Chromium Ions with Methane in the Gas Phase. *J. Am. Chem. Soc.* **1981,** *103*, 962-963.
8. Mandich, M. L.; Halle, L. F.; Beauchamp, J. L., Determination of the Metal-Hydrogen and Metal-methyl Bond Dissociation Energies of the Second Row Group 8 Transition Metal Cations. *J. Am. Chem. Soc.* **1984,** *106*, 4403-4411.
9. Aristov, N.; Armentrout, P. B., Methane Activation by V^+: Electronic and Translational Energy Dependence. *J. Phys. Chem.* **1987,** *91*, 6178-6188.
10. Sunderlin, L. S.; Armentrout, P. B., Methane Activation by Ti^+: Electronic and Translational Energy Dependence. *J. Phys. Chem.* **1988,** *92*, 1209-1219.
11. Georgiadis, R.; Armentrout, P. B., Translational and Electronic Energy Dependence of Chromium Ion Reactions with Methane. *J. Phys. Chem.* **1988,** *92*, 7067-7074.
12. Schultz, R. H.; Elkind, J. L.; Armentrout, P. B., Electronic Effects in C-H and C-C Bond Activation: State-specific Reactions of $Fe^+(^6D, ^4F)$ with Methane, Ethane and Propane. *J. Am. Chem. Soc.* **1988,** *110*, 411-423.
13. Buckner, S. W.; MacMahon, T. J.; Byrd, G. D.; Freiser, B. S., Gas-Phase Reactions of Nb^+ and Ta^+ with Alkanes and Alkenes. C-H Bond Activation and Ligand-Coupling Mechanisms. *Inorg. Chem.* **1989,** *28*, 3511-3518.
14. Irikura, K. K.; Beauchamp, J. L., Osmium Tetroxide and Its Fragment Ions in the Gas Phase: Reactivity with Hydrocarbons and Small Molecules. *J. Am. Chem. Soc.* **1989,** *111*, 75-85.
15. Sunderlin, L. S.; Armentrout, P. B., Periodic Trends in Chemical Reactivity: Reactions of Sc^+, Y^+, La^+, and Lu^+ with Methane and Ethane. *J. Am. Chem. Soc.* **1989,** *111*, 3845-3855.
16. Irikura, K. K.; Beauchamp, J. L., Electronic Structure Considerations for Methane Activation by Third-row Transition-metal Ions. *J. Phys. Chem.* **1991,** *95*, 8344-8351.
17. Irikura, K. K.; Beauchamp, J. L., Methane Oligomerization in the Gas Phase by Third-Row Transition-Metal Ions. *J. Am. Chem. Soc.* **1991,** *113*, 2769-2770.
18. Heinemann, C.; Wesendrup, R.; Schwarz, H., Pt^+-Mediated Activation of Methane: Theory and Experiment. *Chem. Phys. Lett.* **1995,** *239*, 75-83.
19. Van Koppen, P. A. M.; Kemper, P. R.; Bushnell, J. E.; Bowers, M. T., Methane Dehydrogenation by Ti^+: A Cluster-Assisted Mechanism for σ-Bond Activation. *J. Am. Chem. Soc.* **1995,** *117* (7), 2098-2099.
20. Haynes, C. L.; Chen, Y.-M.; Armentrout, P. B., The Potential Energy Surface for Activation of Methane by Co^+: An Experimental Study. *J. Phys. Chem.* **1995,** *99*, 9110-9117.
21. Chen, Y.-M.; Armentrout, P. B., Activation of Methane by Gas-Phase Rh^+. *J. Phys. Chem.* **1995,** *99*, 10775-10779.
22. Haynes, C. L.; Chen, Y.-M.; Armentrout, P. B., The Reaction of $FeCH_2^+ + D_2$: Probing the $[FeCH_4]^+$ Potential Energy Surface. *J. Phys. Chem.* **1996,** *100*, 111-119.
23. Schröder, D.; Schwarz, H.; Clemmer, D. E.; Chen, Y.; Armentrout, P. B.; Baranov, V. I.; Bohme, D. K., Activation of hydrogen and methane by thermalized FeO^+ in the gas phase as studied by multiple mass spectrometric techniques. *Int. J. Mass Spectrom. Ion Process.* **1997,** *161*, 175-191.
24. Chen, Y.-M.; Sievers, M. R.; Armentrout, P. B., Activation of CH_4, C_2H_6, C_3H_8, and c-C_3H_6 by Gas-phase Pd^+ and the Thermochemistry of Pd-ligand Complexes. *Int. J. Mass Spectrom. Ion Processes* **1997,** *167/168*, 195-212.

25. Pavlov, M.; Blomberg, M. R. A.; Siegbahn, P. E. M.; Wesendrup, R.; Heinemann, C.; Schwarz, H., Pt^+-Catalyzed Oxidation of Methane: Theory and Experiment. *J. Phys. Chem. A* **1997,** *101*, 1567-1579.
26. Sievers, M. R.; Chen, Y.-M.; Haynes, C. L.; Armentrout, P. B., Activation of CH_4, C_2H_6, and C_3H_8 by Gas-Phase Nb^+ and the Thermochemistry of Nb-ligand Complexes. *Int. J. Mass Spectrom.* **2000,** *195/196*, 149-170.
27. Zhang, X.-G.; Liyanage, R.; Armentrout, P. B., The Potential Energy Surface for Activation of Methane by Pt^+: A Detailed Guided-Ion Beam Study. *J. Am. Chem. Soc.* **2001,** *123*, 5563-5575.
28. Simon, A.; MacAleese, L.; Boissel, P.; Maître, P., Towards the Characterization of the Mechanism of the Sequential Activation of Four Methane Molecules by Ta^+. *Int. J. Mass Spectrom.* **2002,** *219*, 457-473.
29. Armentrout, P. B.; Sievers, M. R., Activation of CH_4 by Gas-phase Zr^+ and the Thermochemistry of Zr ligand Complexes. *J. Phys. Chem. A* **2003,** *107*, 4396-4406.
30. Armentrout, M. M.; Li, F.-X.; Armentrout, P. B., Is Spin Conserved in Heavy Metal Systems? Experimental and Theoretical Studies of the Reaction of Re^+ with Methane. *J. Phys. Chem. A* **2004,** *108*, 9660-9672.
31. Liu, F.; Zhang, X.-G.; Armentrout, P. B., Activation of CH_4 by Gas-phase Ni^+ and the Thermochemistry of Ni Ligand Complexes. *Phys. Chem. Chem. Phys.* **2005,** *7*, 1054-1064.
32. Armentrout, P. B., Activation of CH_4 by Gas-phase Mo^+ and the Thermochemistry of Mo-ligand Complexes. *J. Phys. Chem. A* **2006,** *110*, 8327-8338.
33. Li, F.-X.; Armentrout, P. B., Activation of Methane by Gold Cations: Guided Ion Beam and Theoretical Studies. *J. Chem. Phys.* **2006,** *125*, 133114
34. Parke, L. G.; Hinton, C. S.; Armentrout, P. B., Why is Hafnium So Unreactive? Experimental and Theoretical Studies of the Reaction of Hf^+ with Methane. *Int. J. Mass Spectrom.* **2006,** *254*, 168-182.
35. Armentrout, P. B.; Shin, S.; Liyanage, R., Guided-Ion Beam and Theoretical Study of the Potential Energy Surface for Activation of Methane by W^+ *J. Phys. Chem. A* **2006,** *110*, 1242-1260.
36. Li, F.-X.; Zhang, X.-G.; Armentrout, P. B., The Most Reactive Third-row Transition Metal: Guided Ion Beam and Theoretical Studies of the Activation of Methane by Ir^+. *Int. J. Mass Spectrom.* **2006,** *255/256*, 279-300.
37. Parke, L. G.; Hinton, C. S.; Armentrout, P. B., Experimental and Theoretical Studies of the Activation of Methane by Ta^+ and the Bond Energies of Ta^+-CH_x (x = 1 - 3). *J. Phys. Chem. C* **2007,** *111*, 17773-17787.
38. Parke, L. G.; Hinton, C. S.; Armentrout, P. B., Energetics and Mechanisms of C-H Bond Activation by a Doubly-charged Metal Ion: Guided Ion Beam and Theoretical Studies of Ta^{2+} + CH_4. *J. Phys. Chem. A* **2008,** *112*, 10469–10480.
39. Marçalo, J.; Santos, M.; Matos, A. P. d.; Gibson, J. K.; Haire, R. G., Gas-Phase Reactions of Doubly Charged Lanthanide Cations with Alkanes and Alkenes. Trends in Metal(2+) Reactivity. *J. Phys. Chem. A* **2008,** *112* (49), 12647-12656.
40. Shayesteh, A.; Lavrov, V. V.; Koyanagi, G. K.; Bohme, D. K., Reactions of Atomic Cations with Methane: Gas Phase Room-Temperature Kinetics and Periodicities in Reactivity. *J. Phys. Chem. A* **2009,** *113*, 5602–5611.
41. Roithová, J.; Schröder, D., Selective Activation of Alkanes by Gas-Phase Metal Ions. *Chem. Rev.* **2010,** *110* (2), 1170–1211.

42. Schwarz, H., Chemistry with Methane: Concepts Rather than Recipes. *Angew. Chem. Int. Ed.* **2011,** *50*, 10096-10115.
43. Armentrout, P. B.; Parke, L.; Hinton, C.; Citir, M., Activation of Methane by Os^+: Guided Ion Beam and Theoretical Studies. *ChemPlusChem* **2013,** *78* (9), 1157-1173.
44. Schwarz, H., How and Why Do Cluster Size, Charge State, and Ligands Affect the Course of Metal-Mediated Gas-Phase Activation of Methane? *Isr. J. Chem.* **2014,** *54*, 1413-1431.
45. Cox, R. M.; Armentrout, P. B.; de Jong, W. A., Activation of CH_4 by Th^+ as Studied by Guided Ion Beam Mass Spectrometry and Quantum Chemistry. *Inorg. Chem.* **2015,** *54* (7), 3584-3599.
46. Armentrout, P. B.; Chen, Y.-M., Activation of Methane by Ru^+: Experimental and Theoretical Studies of the Thermochemistry and Mechanism. *Int. J. Mass Spectrom.* **2017,** *413*, 135-149.
47. Armentrout, P. B., Methane Activation by 5d Transition Metals: Energetics, Mechanisms, and Periodic Trends. *Chem.: Eur. J.* **2017,** *23*, 10-18.
48. Armentrout, P. B.; Kuijpers, S.; Lushchikova, O.; Hightower, R. L.; Boles, G. C.; Bakker, J. M., Spectroscopic Identification of the Carbyne Hydride Structure of the Dehydrogenation Product of Methane Activation by Osmium Cations. *J. Am. Soc. Mass Spectrom.* **2018,** *29*, 1781-1791.
49. Owen, C. J.; Boles, G. C.; Chernyy, V.; Bakker, J. M.; Armentrout, P. B., Structures of the Dehydrogenation Products of Methane Activation by 5d Transition Metal Cations Revisited: Deuterium Labeling and Rotational Contours. *J. Chem. Phys.* **2018,** *148*, 044307.
50. Wheeler, O. W.; Salem, M.; Gao, A.; Bakker, J. M.; Armentrout, P. B., Sequential Activation of Methane by Ir^+: An IRMPD and Theoretical Investigation. *Int. J. Mass Spectrom.* **2019,** *435*, 78-92.
51. Kozubal, J.; Heck, T.; Metz, R. B., Vibrational Spectroscopy of Intermediates and C–H Activation Products of Sequential Zr^+ Reactions with CH_4. *J. Phys. Chem. A* **2020,** *124* (40), 8235-8245.
52. Bakker, J. M.; Owen, C. J.; Nooteboom, S. W.; Lushchikova, O. V.; Armentrout, P. B., Structural characterization of $[M,C,2H]^+$ products formed by reaction of 5d metal cations Pt^+ and Ir^+ with ethylene oxide and Ta^+ with methane using messenger spectroscopy. *J. Mol. Spectrosc.* **2021,** *378*, 111472.
53. Wensink, F. J.; Roos, N.; Bakker, J. M.; Armentrout, P. B., C–H Bond Activation and C–C Coupling of Methane on a Single Cationic Platinum Center: A Spectroscopic and Theoretical Study. *Inorg. Chem.* **2022,** *61* (29), 11252-11260.
54. Armentrout, P. B., Quantitative Aspects of Gas-Phase Metal Ion Chemistry: Conservation of Spin, Participation of f Orbitals, and C–H Activation and C–C Coupling. *J. Phys. Chem. A* **2023,** *127* (46), 9641-9653.
55. Wensink, F. J.; Pradeep, D.; Armentrout, P. B.; Bakker, J. M., IR spectroscopic characterization of products of methane and cyclopropane activation by Ru cations. *Int. J. Mass Spectrom.* **2024,** *495*, 117165.
56. Husband, J.; Aguirre, F.; Thompson, C. J.; Laperle, C. M.; Metz, R. B., Photofragment Spectroscopy of $FeCH_2^+$, $CoCH_2^+$, and $NiCH_2^+$ near the $M^+{-}CH_2$ Dissociation Threshold. *J. Phys. Chem. A* **2000,** *104* (10), 2020-2024.
57. Aguirre, F.; Husband, J.; Thompson, C. J.; Metz, R. B., Gas-phase Photodissociation of $AuCH_2^+$: The Dissociation Threshold of Jet-cooled and Rotationally Thermalized Ions. *Chem. Phys. Lett.* **2000,** *318* (4–5), 466-470.

58. Lapoutre, V. J. F.; Redlich, B.; van der Meer, A. F. G.; Oomens, J.; Bakker, J. M.; Sweeney, A.; Mookherjee, A.; Armentrout, P. B., Structures of the Dehydrogenation Products of Methane Activation by 5d Transition Metal Cations. *J. Phys Chem. A* **2013,** *117*, 4115-4126.
59. Wheeler, O. W.; Salem, M.; Gao, A.; Bakker, J. M.; Armentrout, P. B., Activation of C-H bonds in $Pt^+ + xCH_4$ Reactions, Where x = 1 – 4: Identification of the Platinum Dimethyl Cation. *J. Phys. Chem. A* **2016,** *120*, 6216–6227.
60. Armentrout, P. B.; Stevenson, B. C.; Yang, F.; Wensink, F. J.; Lushchikova, O. V.; Bakker, J. M., Infrared Spectroscopy of Gold Carbene Cation ($AuCH_2^+$): Covalent or Dative Bonding? *J. Phys. Chem. A* **2019,** *123*, 8932-8941.
61. Wensink, F. J.; Smink, C. E.; Bakker, J. M.; Armentrout, P. B., IR spectroscopic characterization of 3d transition metal carbene cations, $FeCH_2^+$ and $CoCH_2^+$: A failure of DFT approaches. *Phys. Chem. Chem. Phys.* **2024,** *26*, 9948 – 9962.
62. Wensink, F. J.; Smink, C. E.; Stevenson, B. C.; Steele, R. P.; Armentrout, P. B.; Bakker, J. M., IR spectroscopic characterization of $[M,C,2H]^+$ (M = Ru and Rh) products formed by reacting 4d transition metal cations with oxirane: Spectroscopic evidence for multireference character in $RhCH_2^+$. *Phys. Chem. Chem. Phys.* **2024,** *26*, 11445-11458.
63. Armentrout, P. B.; Lushchikova, O. V.; Schuurman, J. L.; Nooteboom, S.; Ghiassee, M.; Boles, G. C.; Bakker, J. M., Infrared Spectroscopic Characterization of Early 4d Transition Metal Carbene Cations, $ZrCH_2^+$ and $NbCH_2^+$. *J. Phys. Chem. A* **2024,** *128* (32), 6658-6667.
64. Bubas, A. R.; Walker, S. K.; Wensink, F. J.; Bakker, J. M.; Armentrout, P. B., Activation, Dehydrogenation, and Carbon–Carbon Coupling of Methane by Iridium Cations Studied by Infrared Multiple Photon Dissociation Spectroscopy and Density Functional Theory. *J. Phys. Chem. A* **2025,** *129* (25), 5557-5569.
65. Armentrout, P. B.; Poetsma, B.; Loertscher, D. H.; Kumar, S.; Bakker, J. M., Structures of species formed by sequential methane activation by Ta^+: Infrared multiple photon dissociation spectroscopy and ab Initio calculations. *Int. J. Mass Spectrom.* **2025,** *518*, 117525.
66. Das, A.; Gerrior, J. R.; Metz, R. B., Vibrational Spectroscopy of C–H Activation Intermediates and Dehydrogenation Products of Sequential Reactions of Niobium Cation with Methane. *J. Phys. Chem. A* **2025,** *129* (36), 8407-8418.
67. Bubas, A. R.; French, A. D.; Melby, K. M.; Rodriguez, M. J.; Cox, R. M., An inductively coupled plasma tandem mass spectrometry investigation of the activation of methane by lanthanide cations. *Phys. Chem. Chem. Phys.* **2025,** *27* (18), 9781-9793.
68. Choppin, G. R., Actinide speciation in the environment. *J. Radioanal. Nucl. Chem.* **2007,** *273* (3), 695-703.
69. Almeida, K. J. d.; Duarte, H. A., Gas-Phase Methane Activation by the Ac^+−Pu^+ Ions: Theoretical Insights into the Role of 5f Electrons/Orbitals in Early Actinide Chemistry. *Organomet.* **2009,** *28*, 3203-3211.
70. Gibson, J. K.; Haire, R. G.; Marçalo, J.; Santos, M.; Pires de Matos, A.; Mrozik, M. K.; Pitzer, R. M.; Bursten, B. E., Gas-Phase Reactions of Hydrocarbons with An^+ and AnO^+ (An = Th, Pa, U, Np, Pu, Am, Cm): The Active Role of 5f Electrons in Organoprotactinium Chemistry. *Organomet.* **2007,** *26* (16), 3947-3956.
71. Marçalo, J.; Leal, J. P.; Pires de Matos, A., Gas phase actinide ion chemistry: activation of alkanes and alkenes by thorium cations. *Int. J. Mass Spectrom. Ion Processes* **1996,** *157/158*, 265-274.
72. Di Santo, E.; Michelini, M. d. C.; Russo, N., Methane C−H Bond Activation by Gas-Phase Th^+ and U^+: Reaction Mechanisms and Bonding Analysis. *Organomet.* **2009,** *28* (13), 3716-3726.

73. Di Santo, E.; Santos, M.; Michelini, M. C.; Marçalo, J.; Russo, N.; Gibson, J. K., Gas-Phase Reactions of the Bare Th^{2+} and U^{2+} Ions with Small Alkanes, CH_4, C_2H_6, and C_3H_8: Experimental and Theoretical Study of Elementary Organoactinide Chemistry. *J. Am. Chem. Soc.* **2011,** *133* (6), 1955-1970.
74. Armentrout, P. B.; Hodges, R. V.; Beauchamp, J. L., Metal Atoms as Super Bases: The Gas Phase Proton Affinity of Uranium. *J. Am. Chem. Soc.* **1977,** *99*, 3162-3263.
75. Bubas, A. R.; French, A. D.; Melby, K. M.; Rodriguez, M. J.; Cox, R. M., The balance of orbital overlap and orbital energy in the activation of methane by actinide cations: insights from inductively coupled plasma tandem mass spectrometry. *Inorganic Chemistry Frontiers* **2025,** *12* (4), 1503-1516.
76. Ervin, K. M.; Armentrout, P. B., Translational Energy Dependence of $Ar^+ + XY \rightarrow ArX^+ + Y$ (XY = H_2, D_2, HD) from Thermal to 30 eV c.m. *J. Chem. Phys.* **1985,** *83* (1), 166-189.
77. Loh, S. K.; Hales, D. A.; Lian, L.; Armentrout, P. B., Collision-Induced Dissociation of Fe_n^+ (n = 2 - 10) with Xe: Ionic and Neutral Iron Cluster Binding Energies. *J. Chem. Phys.* **1989,** *90*, 5466-5485.
78. Schultz, R. H.; Armentrout, P. B., Reactions of N_4^+ with Rare Gases from Thermal to 10 eV c.m.: Collision-Induced Dissociation, Charge Transfer, and Ligand Exchange. *Int. J. Mass Spectrom. Ion Processes* **1991,** *107*, 29-48.
79. Taylor, W. S.; Everett, W. R.; Babcock, L. M.; McNeal, T. L., Application of a sputtering glow discharge ion source to a flowing afterglow study of transition metal ion chemistry. *Int. J. Mass Spectrom.* **1993,** *125*, 45-54.
80. Clemmer, D. E.; Chen, Y.-M.; Khan, F. A.; Armentrout, P. B., State-Specific Reactions of $Fe^+(a^6D, a^4F)$ with D_2O and Reactions of FeO^+ with D_2. *J. Phys. Chem.* **1994,** *98*, 6522-6529.
81. Haynes, C. L.; Armentrout, P. B., Thermochemistry and Structures of $CoC_3H_6^+$: Metallacycle and Metal-Alkene Isomers. *Organomet.* **1994,** *13*, 3480-3490.
82. Kickel, B. L.; Armentrout, P. B., Reactions of Fe^+, Co^+ and Ni^+ with Silane. Electronic State Effects, Comparison to Reactions with Methane, and M^+-SiH_x (x = 0 - 3) Bond Energies. *J. Am. Chem. Soc.* **1995,** *117*, 764-773.
83. Kickel, B. L.; Armentrout, P. B., Guided Ion Beam Studies of the Reactions of Mn^+, Cu^+, and Zn^+ with Silane. M^+-SiH_x (x = 0 - 3) Bond Energies. *J. Phys. Chem* **1995,** *99*, 2024-2032.
84. Kickel, B. L.; Armentrout, P. B., Guided Ion Beam Studies of the Reactions of Group 3 Metal Ions (Sc^+, Y^+, La^+, and Lu^+) with Silane. Electronic State Effects, Comparison to Reactions with Methane, and M^+-SiH_x (x = 0 - 3) Bond Energies. *J. Am. Chem. Soc.* **1995,** *117*, 4057-4070.
85. Chen, Y.-M.; Elkind, J. L.; Armentrout, P. B., Reactions of Ru^+, Rh^+, Pd^+, and Ag^+ with H_2, HD and D_2. *J. Phys. Chem.* **1995,** *99*, 10438-10445.
86. Sievers, M. R.; Chen, Y.-M.; Elkind, J. L.; Armentrout, P. B., Reactions of Y^+, Zr^+, Nb^+, and Mo^+ with H_2, HD, and D_2. *J. Phys. Chem.* **1996,** *100*, 54-62.
87. Sansonetti, J. E.; Martin, W. C., Handbook of Basic Atomic Spectroscopic Data. *J. Phys. Chem. Ref. Data* **2005,** *34* (4), 1559-2259.
88. Blaise, J.; Wyart, J.-F. Energy Levels and Atomic Spectra of Actinides *International Tables of Selected Constants 20* [Online], 1992.
89. Zhang, W.-J.; Demireva, M.; Kim, J.; de Jong, W. A.; Armentrout, P. B., Reactions of U^+ with H_2, D_2, and HD Studied by Guided Ion Beam Tandem Mass Spectrometry and Theory. *J. Phys. Chem. A* **2021,** *125* (36), 7825-7839.
90. Teloy, E.; Gerlich, D., Integral Cross Sections for Ion-Molecule Reactions. 1. The Guided Beam Technique. *Chem. Phys.* **1974,** *4*, 417-427.

91. Gerlich, D., Inhomogeneous rf Fields: A Versatile Tool for the Study of Processes with Slow Ions. *Adv. Chem. Phys.* **1992,** *82*, 1-176.
92. Daly, N. R., Scintillation Type Mass Spectrometer Ion Detector. *Rev. Sci. Instrum.* **1960,** *31*, 264-267.
93. Weber, M. E.; Elkind, J. L.; Armentrout, P. B., Kinetic Energy Dependence of $Al^+ + O_2 \rightarrow AlO^+ + O$. *J. Chem. Phys.* **1986,** *84*, 1521-1529.
94. Frisch, M. J.; Trucks, G. W.; Schlegel, H. B.; Scuseria, G. E.; Robb, M. A.; Cheeseman, J. R.; Scalmani, G.; Barone, V.; Petersson, G. A.; Nakatsuji, H.; Li, X.; Caricato, M.; Marenich, A. V.; Bloino, J.; Janesko, B. G.; Gomperts, R.; Mennucci, B.; Hratchian, H. P.; Ortiz, J. V.; Izmaylov, A. F.; Sonnenberg, J. L.; Williams-Young, D.; Ding, F.; Lipparini, F.; Egidi, F.; Goings, J.; Peng, B.; Petrone, A.; Henderson, T.; Ranasinghe, D.; Zakrzewski, V. G.; Gao, J.; Rega, N.; Zheng, G.; Liang, W.; Hada, M.; Ehara, M.; Toyota, K.; Fukuda, R.; Hasegawa, J.; Ishida, M.; Nakajima, T.; Honda, Y.; Kitao, O.; Nakai, H.; Vreven, T.; Throssell, K.; J. A. Montgomery, J.; Peralta, J. E.; Ogliaro, F.; Bearpark, M. J.; Heyd, J. J.; Brothers, E. N.; Kudin, K. N.; Staroverov, V. N.; Keith, T. A.; Kobayashi, R.; Normand, J.; Raghavachari, K.; Rendell, A. P.; Burant, J. C.; Iyengar, S. S.; Tomasi, J.; Cossi, M.; Millam, J. M.; Klene, M.; Adamo, C.; Cammi, R.; Ochterski, J. W.; Martin, R. L.; Morokuma, K.; Farkas, O.; Foresman, J. B.; Fox, D. J. *Gaussian 16, Revision A.03*, Gaussian, Inc.: Wallingford CT, 2016.
95. Peterson, K. A., Correlation consistent basis sets for actinides. I. The Th and U atoms. *J. Chem. Phys.* **2015,** *142* (7), 074105.
96. Weigand, A.; Cao, X.; Hangele, T.; Dolg, M., Relativistic Small-Core Pseudopotentials for Actinium, Thorium, and Protactinium. *J. Phys. Chem. A* **2014,** *118* (13), 2519-2530.
97. Pritchard, B. P.; Altarawy, D.; Didier, B.; Gibson, T. D.; Windus, T. L., A New Basis Set Exchange: An Open, Up-to-date Resource for the Molecular Sciences Community. *J. Chem. Inf. Model.* **2019,** *59* (11), 4814-4820.
98. Karton, A.; Martin, J. M. L., Comment on: "Estimating the Hartree–Fock limit from finite basis set calculations" [Jensen F (2005) Theor Chem Acc 113:267]. *Theor. Chem. Acct.* **2006,** *115* (4), 330-333.
99. Martin, J. M. L., Ab initio Total Atomization Energies of Small Molecules - Towards the Basis Set Limit. *Chem. Phys. Lett.* **1996,** *259*, 669-678.
100. Feller, D.; Peterson, K. A.; Hill, J. G., On the effectiveness of CCSD(T) complete basis set extrapolations for atomization energies. *J. Chem. Phys.* **2011,** *135* (4), 044102.
101. Roos, B. O.; Taylor, P. R.; Sigbahn, P. E. M., A complete active space SCF method (CASSCF) using a density matrix formulated super-CI approach. *Chem. Phys.* **1980,** *48* (2), 157-173.
102. Sauri, V.; Serrano-Andrés, L.; Shahi, A. R. M.; Gagliardi, L.; Vancoillie, S.; Pierloot, K., Multiconfigurational Second-Order Perturbation Theory Restricted Active Space (RASPT2) Method for Electronic Excited States: A Benchmark Study. *J. Chem. Theory Comput.* **2011,** *7* (1), 153-168.
103. Malmqvist, P. Å.; Roos, B. O.; Schimmelpfennig, B., The restricted active space (RAS) state interaction approach with spin–orbit coupling. *Chem. Phys. Lett.* **2002,** *357* (3), 230-240.
104. Bross, D. H.; Peterson, K. A., Theoretical spectroscopy study of the low-lying electronic states of UX and UX^+, X = F and Cl. *J. Chem. Phys.* **2015,** *143* (18), 184313.
105. Antonov, I. O.; Heaven, M. C., Spectroscopic and Theoretical Investigations of UF and UF^+. *J. Phys. Chem. A* **2013,** *117* (39), 9684-9694.

106. Dolg, M.; Cao, X., Accurate Relativistic Small-Core Pseudopotentials for Actinides. Energy Adjustment for Uranium and First Applications to Uranium Hydride. *J. Phys. Chem. A* **2009,** *113* (45), 12573-12581.
107. Burley, J. D.; Ervin, K. M.; Armentrout, P. B., Translational Energy Dependence of $O^+(^4S)$ + $H_2(D_2, HD) \rightarrow OH^+(OD^+)$ + H(D) from Thermal to 30 eV c.m. *Int. J. Mass Spectrom. Ion Processes* **1987,** *80*, 153-175.
108. Ruscic, B.; Bross, D. H. Active Thermochemical Tables (ATcT) values based on ver. 1.130 of the Thermochemical Network. available at ATcT.anl.gov (accessed 2/12/24).
109. Kramida, A.; Ralchenko, Y.; Reader, J.; Team, N. A. NIST Atomic Spectra Database (ver. 5.7.1), [Online]. Available: http://physics.nist.gov/asd 2012. (accessed Nov 1, 2019).
110. Zhang, W.; Hunt, A. R. E.; Kim, J. S.; Demireva, M.; Peterson, K. A.; Armentrout, P. B., Bond Energies of UO^+ and UC^+: Guided Ion Beam and Quantum Chemical Studies of the Reactions of Uranium Cation with O_2 and CO. *Isr. J. Chem.* **2023,** *63* (7-8), e202300026.
111. Berkowitz, J.; Ellison, G. B.; Gutman, D., Three Methods To Measure RH Bond Energies. *J. Phys. Chem.* **1994,** *98*, 2744-2765.
112. Feller, D.; Peterson, K. A.; Dixon, D. A., A Survey of Factors Contributing to Accurate Theoretical Predictions of Atomization Energies and Molecular Structures. *J. Chem. Phys.* **2008,** *129* (20), 204105.
113. de Melo, G. F.; Vasiliu, M.; Marshall, M.; Zhu, Z.; Tufekci, B. A.; Ciborowski, S. M.; Blankenhorn, M.; Harris, R. M.; Bowen, K. H.; Dixon, D. A., Experimental and Computational Description of the Interaction of H and H– with U. *J. Phys. Chem. A* **2022,** *126* (27), 4432-4443.
114. de Melo, G. F.; Vasiliu, M.; Liu, G.; Ciborowski, S.; Zhu, Z.; Blankenhorn, M.; Harris, R.; Martinez-Martinez, C.; Dipalo, M.; Peterson, K. A.; Bowen, K. H.; Dixon, D. A., Theoretical and Experimental Study of the Spectroscopy and Thermochemistry of UC(+/0/). *J. Phys. Chem. A* **2022,** *126* (50), 9392-9407.
115. Cox, R. M.; Armentrout, P. B.; de Jong, W. A., Reactions of $Th^+ + H_2$, D_2, and HD Studied by Guided Ion Beam Tandem Mass Spectrometry and Quantum Chemical Calculations. *J. Phys. Chem. B* **2016,** *120*, 1601-1614.
116. Foster, J. P.; Weinhold, F., Natural Hybrid Orbitals. *J. Am. Chem. Soc.* **1980,** *102* (24), 7211-7218.
117. Glendening, E. D.; Reed, A. E.; Carpenter, J. E.; Weinhold, F. *NBO Version 3.1*, Gaussian Inc.: Pittsburgh, 2003.
118. Linstrom, P. J.; Mallard, W. G., *NIST Chemistry WebBook, NIST Standard Reference Database Number 69*. National Institute of Standards and Technology: Gaithersburg MD, 20899, 2003; Vol. (http://webbook.nist.gov).
119. Marçalo, J.; Gibson, J. K., Gas-Phase Energetics of Actinide Oxides: An Assessment of Neutral and Cationic Monoxides and Dioxides from Thorium to Curium. *J. Phys. Chem. A* **2009,** *113* (45), 12599-12606.

Table 1. Fitting parameters from Equation 1 for reactions of $U^+ + CH_4$. Values in parentheses correspond to the $U^+ + CD_4$ reaction.

Products	σ_0	n	E_0 (eV)	D_0 (eV)	p	E_d (eV)
$UH^+ + CH_3$	8.24 ± 0.40 (5.02 ± 0.30)	1.3 ± 0.2 (1.4 ± 0.1)	2.11 ± 0.15 (2.10 ± 0.13)	2.37 ± 0.15 (2.48 ± 0.13)	-	-
$UC^+ + 2\ H_2$[a]	0.32 ± 0.10 (0.30 ± 0.10)	2.7 ± 0.2 (1.5 ± 0.2)	4.12 ± 0.10 (4.26 ± 0.12)	3.94 ± 0.10 (3.95 ± 0.12)	2	6.3
$UCH^+ + H_2$ + H	0.52 ± 0.10 (0.88 ± 0.08)	0.40 ± 0.14 (0.9 ± 0.2)	4.32 ± 0.16 (4.26 ± 0.10)	4.75 ± 0.16 (4.99 ± 0.10)	-	-
$UCH_2^+ + H_2$	4.12 ± 0.20 (2.98 ± 0.3)	1.5 ± 0.2 (1.8 ± 0.2)	0.63 ± 0.05 (0.68 ± 0.06)	4.11 ± 0.05 (4.14 ± 0.06)	3	2.28
$UCH_3^+ + H$	0.47 ± 0.10 (0.36 ± 0.05)	1.1 ± 0.1 (1.4 ± 0.2)	2.11 ± 0.12 (2.09 ± 0.15)	2.37 ± 0.12 (2.49 ± 0.15)	4	4.12

[a] These cross sections were analyzed after accounting for the decline in the UCH_2^+ (UCD_2^+) precursor.

Table 2. Theoretical and Experimental bond dissociation energies (eV) for all products

	Theory		Experiment		
Bond	Russo[a]	B3LYP[b,c]	CCSD(T)[c,d]	GIBMS[e]	ICP-MS/MS[f]
U^+ - H	2.35	2.61 (2.53)[g]	2.48 (2.41)[g] 2.44 ± 0.05[h]	2.42 ± 0.10 2.48 ± 0.06 [g]	2.61 ± 0.37
U^+ - CH_3	2.42	2.67 (2.51)	2.72 (2.56)	2.41 ± 0.09	3.02 ± 0.34
U^+ - CH_2	3.90	3.81 (3.50)	3.98 (3.67)	4.11 ± 0.04	3.62 ± 0.35
U^+ - CH		4.51 (4.33)	4.90 (4.72)	4.91 ± 0.09	5.91 ± 0.35
U^+ - C		3.82 (3.62) [i]	4.02 (3.82) [i] 4.10 [j]	3.95 ± 0.12 4.03 ± 0.13 [k]	4.74 ± 0.70

[a] B3LYP/SDD results from Russo and coworkers, ref. [72]. [b] UB3LYP/CBS// UB3LYP/cc-pwCVTZ-MDF/aug-cc-pCVXZ/aug-cc-pVTZ level of theory. [c] Values in parentheses correspond to the spin-orbit corrected energy. [d] UCCSD(T)/CBS//UB3LYP/VTZ. [e] This work except as noted. [f] Results from Bubas et al., ref. [75]. [g] Ref. [89]. [h] FPD value from ref. [113]. [i] CBS extrapolations performed here from theoretical results in Ref. [110]. [j] FPD value from ref. [114]. [k] Experimental BDE from ref. [110].

Table 3. Relative energies (kJ/mol) along the quartet spin surface for the reaction of $U^+(^4I)$ with methane at CCSD(T)/CBS//B3LYP/VTZ and B3LYP/CBS//B3LYP/VTZ levels of theory compared with the Russo and co-worker's calculations at the B3LYP/SDD level of theory

Species	CCSD(T)	B3LYP	Russo[a]
U^+ (^4I) + CH_4	0.0	0.0	0.0
$U^+(CH_4)$ INT1 (^4A)	-28.2	-15.5	-21.6
TS1/2 (^4A)	53.3	68.2	57.4
$HUCH_3^+$ INT2 ($^4A'$)	-70.1	-69.3	-78.2
TS2/3 (^4A)	43.5	48.5	36.8
$(H_2)UCH_2^+$ INT3 (^4A)	40.5	49.3	38.7
UCH_2^+ ($^4A''$) + H_2	71.4	83.0	70.9
UCH_3^+ ($^5A_1$) + H	169.0	167.9	158.2
UH^+ (^5I) + CH_3	192.1	174.3	165.6
UCH^+ ($^3A''$) + H_2 + H	398.5	434.8	

[a] Ref. [72].

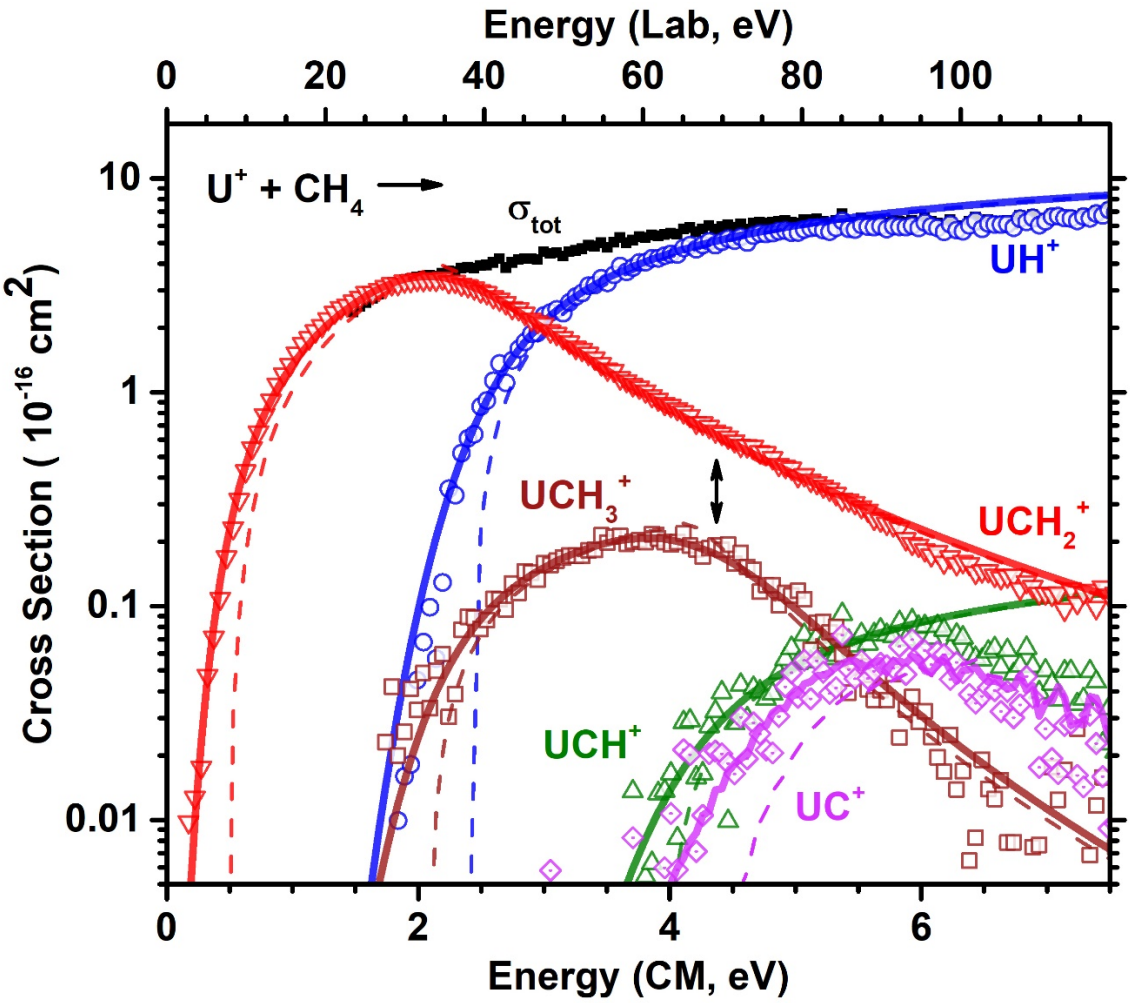

Figure 1. Cross sections (open symbols) for the reaction between U^+ and CH_4 as a function of energy in the center-of-mass (lower x-axis) and laboratory (upper x-axis) frames. The model of equation 1 for each product with parameters from Table 1 is shown as a dashed line and the solid line shows the model convoluted over the kinetic and internal energy distributions of reactants. The vertical arrow indicates $D_0(CH_4)$ at 4.48 eV.

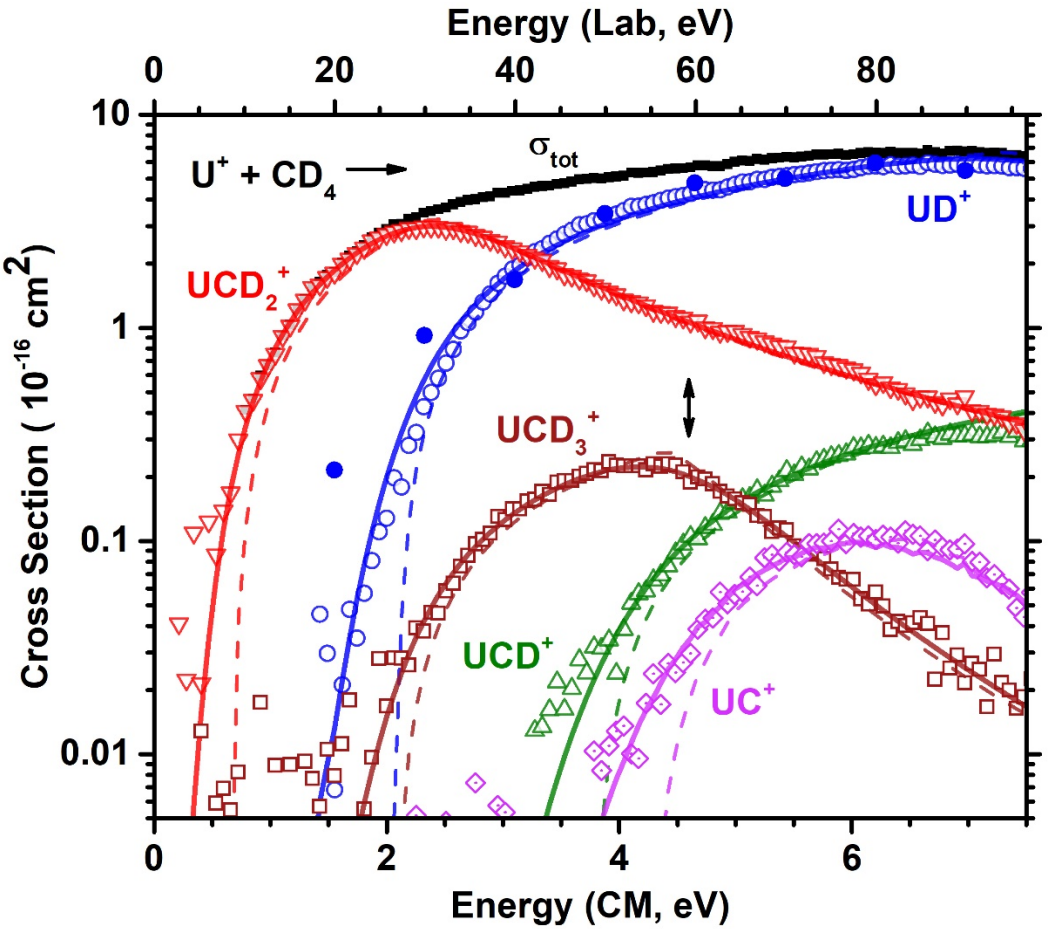

Figure 2. Cross sections (open symbols) for the reaction between U^+ and CD_4 as a function of energy in the center-of-mass (lower x-axis) and laboratory (upper x-axis) frames. The model of equation 1 for each product with parameters from Table 1 is shown as a dashed line and the solid line shows the model convoluted over the kinetic energy and internal energy distributions of reactants. The vertical arrow indicates $D_0(CD_4)$ at 4.58 eV. Solid blue circles show the data from Armentrout and Beauchamp, ref. [6] multiplied by a factor of three.

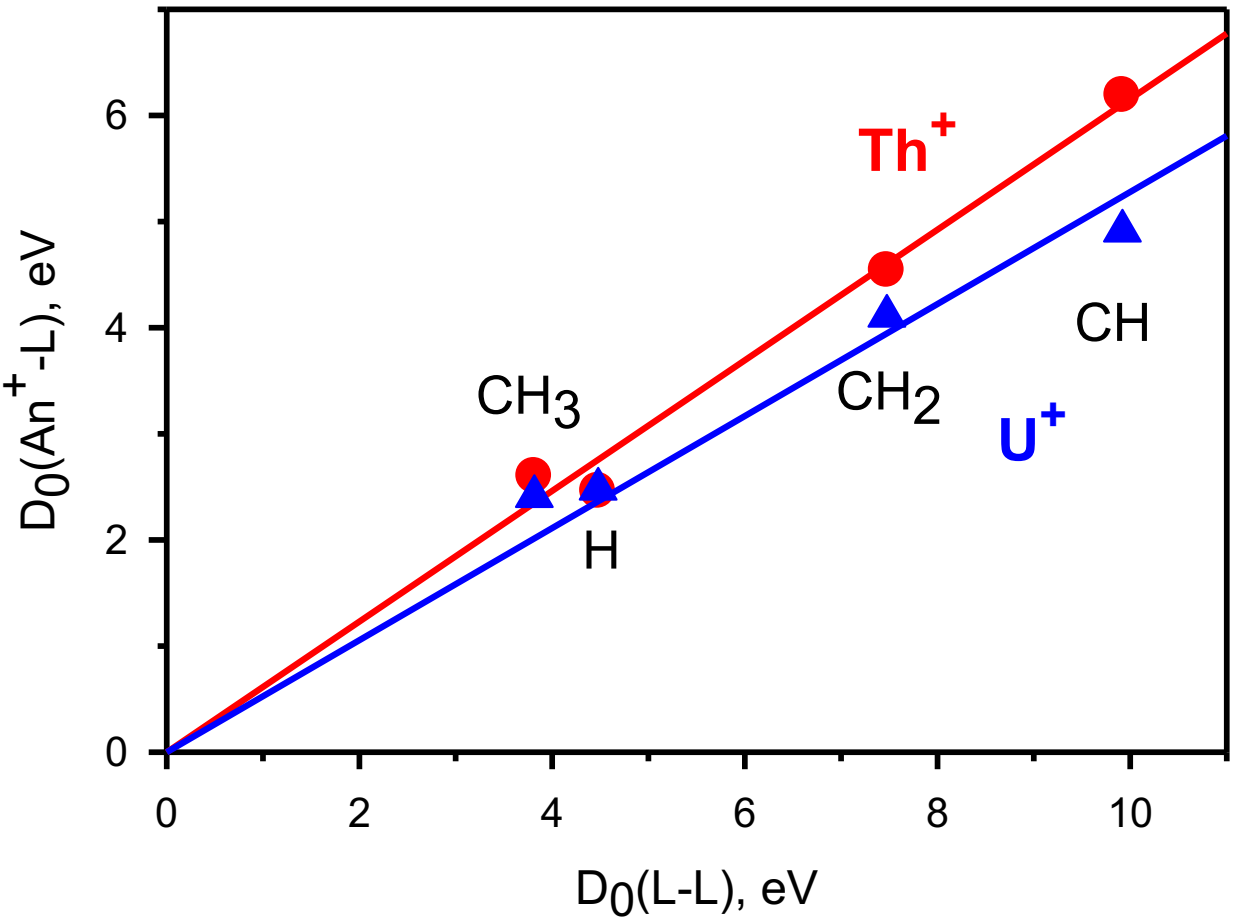

Figure 3. Bond energy-bond order (BEBO) plot between $D_0(An^+–L)$ versus $D_0(L–L)$ where An^+ is Th^+ (red circles) and U^+ (blue triangles). The associated lines are linear regression plots of the data constrained to pass through the origin.

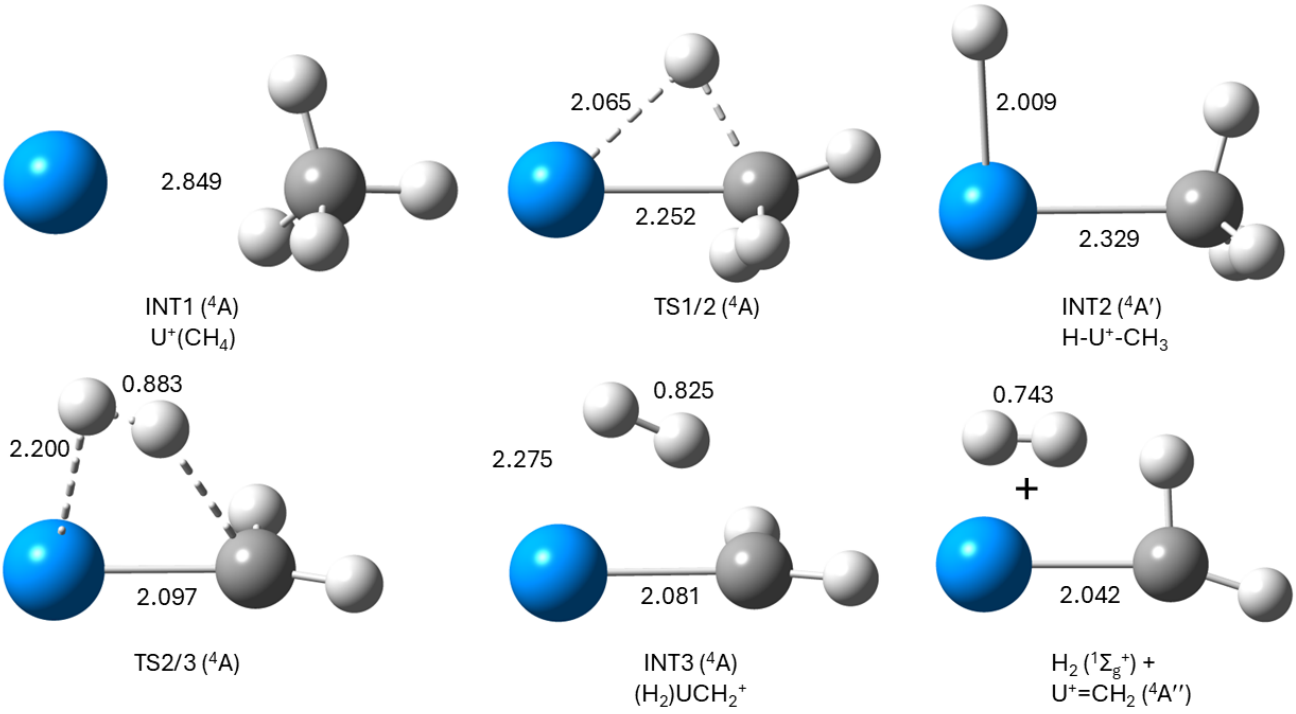

Figure 4. Structures of all intermediates and transition states involved in the reaction of U^+ and CH_4 calculated at the B3LYP/VQZ level of theory. UC, UH, and HH bond distances are provided in Å. Dashed lines indicate bonds that are breaking or forming. U – blue; C – grey; H – white.

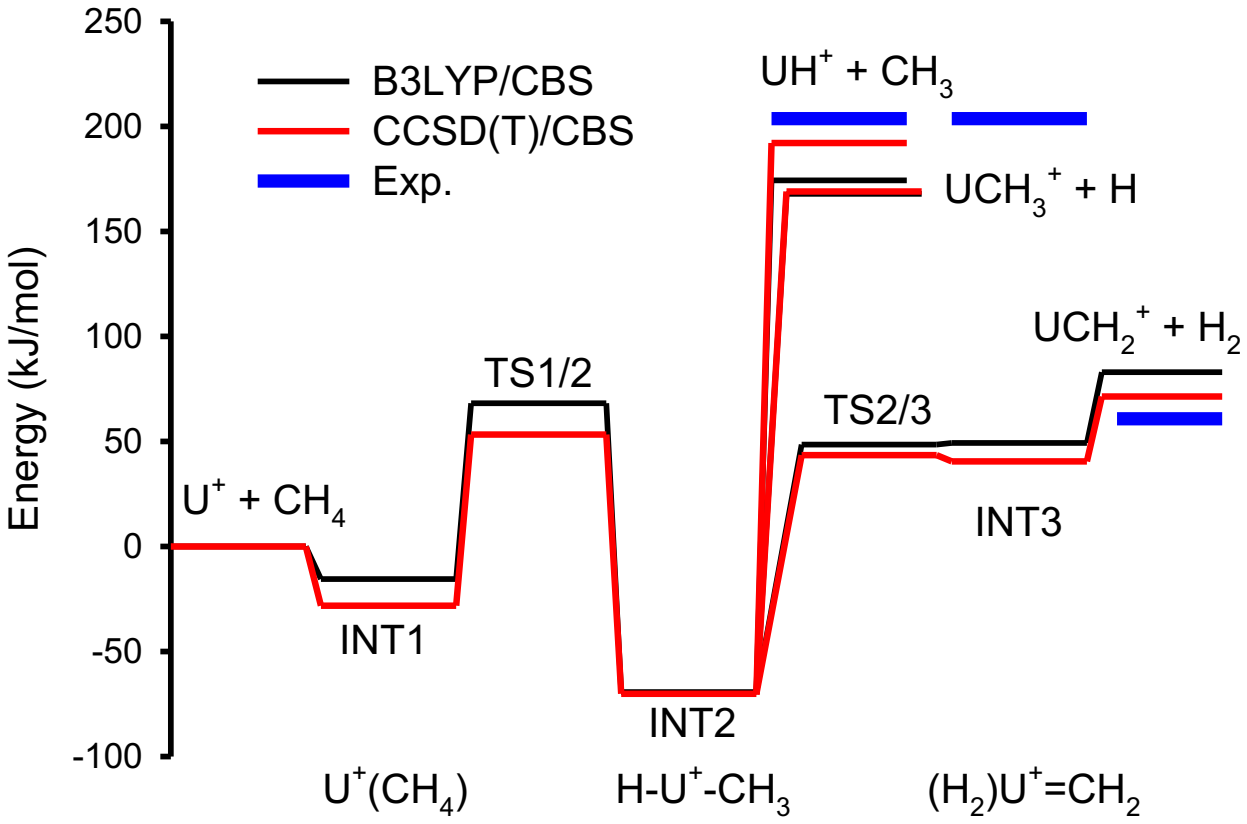

Figure 5. Quartet spin potential energy surface for the reaction of U^+ and methane calculated at the B3LYP/CBS (black lines) and CCSD(T)/CBS//B3LYP/VQZ (red lines) levels of theory. Thick blue lines show experimental values.